ADVANCED MATERIALS
www.advmat.de

Designer Metal–Organic Frameworks for Size-Exclusion-Based Hydrocarbon Separations: Progress and Challenges

*Hao Wang, Yunling Liu, and Jing Li**

The separation of hydrocarbons is of primary importance in the petrochemical industry but remains a challenging process. Hydrocarbon separations have traditionally relied predominantly on costly and energy-intensive heat-driven procedures such as low-temperature distillations. Adsorptive separation based on porous solids represents an alternative technology that is potentially more energy efficient for the separation of some hydrocarbons. Great efforts have been made recently not only in the development of adsorbents with optimal separation performance but also toward the subsequent implementation of adsorption-based separation technology. Emerging as a relatively new class of multifunctional porous materials, metal–organic frameworks (MOFs) hold substantial promise as adsorbents for highly efficient separation of hydrocarbons. This is because of their exceptional and intrinsic porosity tunability, which enables size-exclusion-based separations that render the highest possible separation selectivity. In this review, recent advances in the development of MOFs for separation of selected groups of hydrocarbons are reviewed, including methane/C_2 hydrocarbons, normal alkanes, alkane isomers, and alkane/alkene/alkyne and C_8 alkylaromatics, with a particular focus on separations based on the size-exclusion mechanism. Insights into tailor-made structures, material design strategies, and structure–property relationships will be elucidated. In addition, the existing challenges and possible future directions of this important research field will be discussed.

1. Introduction

Hydrocarbons, in particular, light hydrocarbons with carbon number up to 9, are indispensable resources for fuels, plastics, and polymers. As the largest petroleum fraction, light hydrocarbons are generally produced from oil refinement or natural gas processing, and their demand has continued to increase very rapidly worldwide.[1] For example, ethylene and propylene are the feedstock for manufacturing polyethylene and polypropylene, the world's most and second-most widely produced synthetic plastics, respectively. With an annual growth rate of 4–5%, it is anticipated that the need for polymer-grade ethylene and propylene will follow the same trend.[2] Branched alkanes (C_5-C_7), particularly dibranched isomers, are also in great demand globally as they prove to be ideal components to improve the octane ratings of premium gasoline.[3] However, the current manufacture processes for these hydrocarbons, predominantly catalytic cracking/isomerization reactions, often yield products containing significant amounts of impurities. Thus, the purification of these isomers is essential to meet the minimum purity requirements.

As a crucial industrial process, hydrocarbon separations account for a great portion of global energy consumption.[4] They have traditionally been accomplished by heat-driven procedures such as cryogenic distillations, which are often associated with high cost and tremendous energy input because they typically require strict operating conditions (temperature/pressure) and large numbers of distillation trays. In comparison, adsorptive separation by porous solids at ambient conditions is potentially advantageous with respect to energy input and capital cost, and thus, has been proposed as an alternative separation technology.[5,6] In this context, the development of adsorbent materials with optimal separation efficiency proves vital for the implementation of adsorptive separation technology. Conventional porous solids including zeolites, activated carbons, and porous alumina have been extensively explored for their potential use in the separation of hydrocarbons.[7,8] Zeolites are of notable interest because of their intrinsic structural advantages. They have been utilized in certain industrial separation processes, such as the removal of linear alkanes from their branched isomers (zeolite 5A). However, because of their limited structural diversity and tunability, hydrocarbon separation by zeolites has not been widely implemented as of today, with the traditional heat-driven processes remaining to be the dominating separation technology. This has motivated researchers in academia and engineers in industry to develop novel adsorbent

Prof. H. Wang, Prof. J. Li
Hoffmann Institute of Advanced Materials
Shenzhen Polytechnic
7098 Liuxian Boulevard, Shenzhen, Guangdong 518055, China
Prof. Y. Liu
State Key Laboratory of Inorganic Synthesis & Preparative Chemistry
Jilin University
2699 Qianjin Street, Changchun 130012, China
Prof. J. Li
Department of Chemistry and Chemical Biology
Rutgers University
123 Bevier Road, Piscataway, NJ 08854, USA
E-mail: jingli@rutgers.edu
The ORCID identification number(s) for the author(s) of this article can be found under https://doi.org/10.1002/adma.202002603.

DOI: 10.1002/adma.202002603

materials with high separation performance that could fulfill the requirement of industrial processes.

Development of metal–organic frameworks (MOFs) has been a continuous research hotspot since the late 1990s.[9] MOFs are crystalline porous materials structurally composed of inorganic nodes (metal ions) and organic linkers connected by coordinate bonds. Such materials are potentially useful for catalysis,[10,11] energy storage,[12,13] separation,[14–16] chemical sensing,[17–19] proton conductivity,[20,21] energy efficient lighting technology,[22,23] and other relevant applications.[24–25] Compared to traditional porous materials, MOFs are featured by their exceptionally high surface area (BET surface area up to 7000 m^2 g^{-1}), extraordinary structural diversity, and systematically tunable pore structure and surface functionality.[26] In addition, structural flexibility, observed for each one out of 200 reported compounds, has led to many unique and unexpected properties with dependence on temperature, pressure, or guest species.[27–29] MOFs have shown enormous potential in the aforementioned applications, and hold particular promise as adsorbents for hydrocarbon separations in light of their inherent advantages, including excellent tunability in their pore size, shape, and surface functionality.[14,30–33] By judicious selection of metals and ligands, or by pre- or post-synthetic functionalization of the inorganic nodes or organic linkers, MOFs can be tailored to achieve specific functionality for targeted separations. For example, MOFs with open metal sites (OMSs) generally show preferential adsorption toward olefins over their counterpart paraffins.[34] Furthermore, the application of reticular chemistry would allow us to tune the pore size of MOFs at sub-angstrom level, which is of particular importance to gain optimum separation efficiency.[35,36] The precise control of pore size could be realized through the design of ligands, as well as inorganic secondary building units (SBUs).[37,38] By applying these strategies, reticular chemistry has proven to be a powerful tool to guide the development of MOFs capable of full separation of molecules with dimensional differences less than 0.5 Å.

The separation of hydrocarbons can be generally divided into three categories based on underlying mechanisms: thermodynamically controlled, kinetically controlled, and size-exclusion-based.[39] Thermodynamic separation is commonly observed in MOFs, where the separation originates from differences in adsorption affinities and no significant diffusional restrictions exist for any of the adsorbate. The aforementioned separation of olefins and paraffins by OMSs containing MOFs usually falls into this category. In contrast, kinetically controlled separation on the basis of differences in adsorption rates of each adsorbate is more efficient in cases where the removal or retention of an individual component from a mixture is needed.[40,41] The separation based on molecular size-exclusion, where one or more adsorbates are adsorbed while the others are completely excluded, is considered the most ideal scenario as it offers the highest possible separation selectivity and efficiency among the three separation mechanisms. It should be mentioned that size-exclusion can also be considered as an extreme case of kinetically controlled separation process. By comparison, size-exclusion-based separation is relatively rare because of the stringent requirements for the pore structure (i.e., pore size and shape) of the adsorbents. As for industrial processes, the highly efficient kinetically controlled or size-exclusion separation is more favorable. For instance, the separation of alkane isomers by zeolite 5A[3] and propane/propylene separation by chabazite (CHA) zeolite[40] are based on size-exclusion and kinetic separation, respectively. Beneficial from their high tunability of the pore structures, multiple MOFs have been reported for efficient separation of selected hydrocarbon mixtures by either kinetically controlled or size-exclusion-based

Hao Wang received his B.S. degree from Wuhan University, China, in 2012, and Ph.D. degree from Rutgers University, United States, in 2018. He then joined the Hoffmann Institute of Advanced Materials (HIAM) at Shenzhen Polytechnic, where he is currently an associate professor. His research focuses on the design of novel crystalline porous materials and their applications in adsorption and separation.

Yunling Liu received his Ph.D. from Jilin University in 2000, and then he joined the State Key Laboratory of Inorganic Synthesis and Preparative Chemistry at Jilin University as an assistant professor. He was promoted to associate professor in 2004 and then to full professor in 2008. His research focuses on the design and synthesis of porous functional metal–organic frameworks in gas storage and separation applications.

Jing Li received her Ph.D. degree from Cornell University in 1990 under the guidance of Professor Roald Hoffmann. She joined the chemistry faculty at Rutgers University in 1991 as an assistant professor. She became an associate professor in 1996, full professor in 1999, and distinguished professor in 2006. Her research focuses on designing and developing new and functional materials (including MOFs and hybrid semiconductors) for renewable-, sustainable-, and clean-energy related applications.

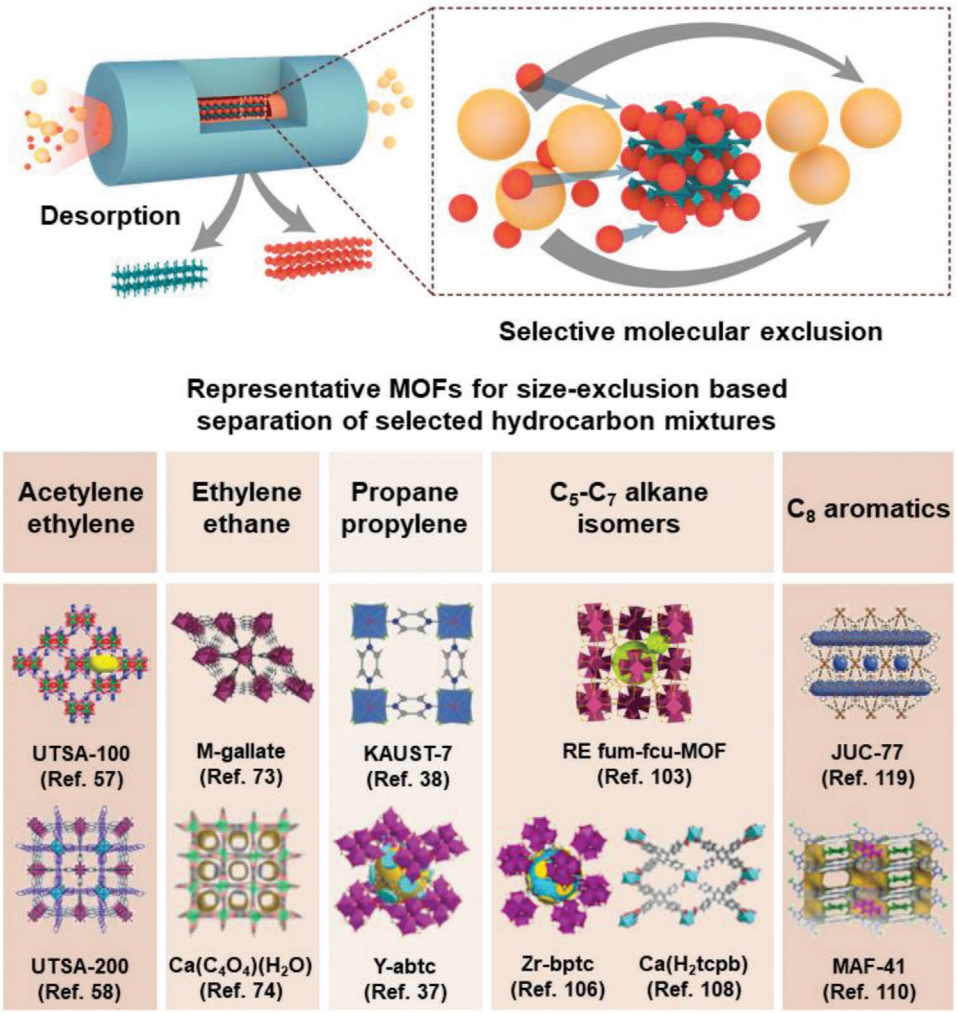

Figure 1. Schematic demonstrating size-exclusion-based separation of hydrocarbons by MOF adsorbent (top) and representative MOF materials for the separation of selected hydrocarbon mixtures (bottom). The corresponding reference for each material is listed.

mechanisms over the past several years (**Figure 1**). In this review article, we highlight the major research progresses in utilizing MOFs for the separation of hydrocarbons, with a specific focus on size-exclusion-based separations. We include not only those cases where complete molecular exclusion occurs, but also highly efficient kinetically driven separations where pore size plays a key role in restricting the diffusion of certain adsorbates, resulting in partial size exclusion. The hydrocarbon systems covered in our discussions are methane/C_2 hydrocarbons, normal alkanes with different carbon numbers, alkane/alkene/alkyne mixtures, C_5–C_7 alkane isomers, and C_8 alkylaromatics (**Table 1**). For each type of separations, we summarize major advantages of the MOFs designed for size-exclusion-based separation and compare them with one to two best-performing MOF materials investigated for thermodynamically driven separation. We emphasize the designability of MOFs to achieve ideal pore structure and optimum separation performance, and the understanding of adsorption/separation mechanisms at the molecular level. In addition to compiling a table of MOFs (**Table 2**) that demonstrate size-exclusion-based hydrocarbon separation (including those classified as kinetic-based separation but can be considered, at least in part, as size-exclusion due to the very high efficiency), we also provide a comprehensive analysis and assessment of selected MOF examples. Finally, we discuss the existing challenges and possible directions for future research in the implementation of MOF-based separation of hydrocarbons.

2. Separation of Normal Alkanes

2.1. Purification of Methane

Methane, the main constituent of natural gas, represents one of the most important energy sources with a high energy density of 55.5 MJ kg^{-1}, and its combustion provides a significant fraction of the world's primary energy. Various impurities, including CO_2 and saturated/unsaturated C_2 and C_3 hydrocarbons, exist in various methane sources and must be separated or removed.[33] The removal of CO_2 from methane is relatively

Table 1. Kinetic diameter and molecular dimensions for selected hydrocarbon molecules[120–122].

Adsorbate	Kinetic diameter [Å]	Molecular dimensions [Å]		
		x	y	z
Methane	3.758	3.829	4.101	3.942
Acetylene	3.3	3.32	3.34	5.70
Ethylene	4.163	3.28	4.18	4.84
Ethane	4.443	3.809	4.079	4.821
Propylene	4.678	6.5	4.0	3.8
Propane	4.3–5.118	6.61	4.52	4.02
n-Hexane	4.3	10.344	4.536	4.014
2-Methylpentane	5.5	9.2	6.4	5.3
3-Methylpentane	5.5	9.3	6.2	5.2
2,2-Dimethylbutane	6.2	8.0	6.7	5.9
2,3-Dimethylbutane	5.8	7.8	6.7	5.3
Benzene	5.349–5.85	6.628	7.337	3.277
Toluene	5.25	6.625	4.012	8.252
Ethylbenzene	5.8	6.625	5.285	9.361
Styrene	5.3	6.7	3.3	9.7
p-Xylene	5.8	6.618	3.810	9.146
o-Xylene	6.8	7.269	3.834	7.826
m-Xylene	6.8	8.994	3.949	7.315

easy as CO_2 has a notably larger quadrupole moment (4.30×10^{26} esu cm^2 vs 0) and polarizability (29.1×10^{25} vs 25.9×10^{25} cm^3) compared to that of methane. This will generally render stronger adsorbate–adsorbent interaction for CO_2. Thus, a number of MOFs, including those with OMSs or polar functional groups (–OH, –NH_2, etc.), have shown preferred CO_2 adsorption over methane with super high selectivity.[42–44] In addition, CO_2 has a smaller molecular size than that of methane (3.3 vs 3.8 Å), which also makes separation based on size differentiation possible. By fine-tuning the pore size/shape of MOFs with reticular chemistry strategy, MOFs with suitable pore structures and capable of size-exclusion-based separation of CO_2 and methane can be achieved. Such examples include $Mn(HCOO)_2$,[45] Qc-5-Cu-sql series,[46] etc.

By comparison, the separation of methane from C_2/C_3 hydrocarbons is more challenging as their molecular sizes and physical properties are similar. However, the separation is of significant importance as it not only produces methane with high purity, but also extracts C_2/C_3 hydrocarbons from methane for further use as important raw materials in chemical industry. Generally, MOFs with OMSs show preferential adsorption toward C_2/C_3 hydrocarbons over methane. A prototype example is MOF-74-Fe,[47] which is built on Fe(II) metal centers and dobdc (dobdc = 2,5-dioxido-1,4-benzenedicarboxylate) linkers. The structure is a 3D framework possessing 1D channels decorated by a high density of Fe(II) OMSs. It adsorbs substantial amount of C_2/C_3 hydrocarbons (i.e., acetylene, ethylene, ethane, and propylene, close to one molecule per Fe) at room temperature and ambient pressure but negligible methane under identical conditions. Multicomponent column breakthrough measurements suggested that C_2/C_3 hydrocarbons could be well-separated from methane by MOF-74-Fe. The selective separation may be attributed to the different extent of adsorption strength between the Fe (II) and the adsorbates. Plonka et al. reported the separation of methane from C_2 hydrocarbons (acetylene, ethylene, and ethane) by two Ca-based microporous MOFs, Ca(sdb) (also termed as SBMOF-1, sdb = 4,4′-sulfonyldibenzoate) and Ca(H_2tcpb) (also termed as SBMOF-2, tcpb = 1,2,4,5-tetrakis(4-carboxyphenyl)-benzene) (**Figure 2**).[48] These two MOFs have relatively small pore sizes of 5–5.5 Å. Gas adsorption measurements revealed that both materials preferentially adsorb C_2 hydrocarbons over methane, with noticeably higher adsorption capacity for the former. Further investigation indicated that the selective adsorption was a result of the size matching between C_2 hydrocarbon molecules and the MOF channels.

2.2. Normal Alkanes with Different Carbon Numbers

Normal alkanes with different carbon numbers have similar kinetic diameters but different lengths. Thus, cage-like or segmented pores, where each cage or segment can accommodate shorter alkanes but exclude longer ones, may be able to discriminate normal alkanes with high efficiency. This has been confirmed by reported studies. MOFs that can separate normal alkanes with different carbon numbers usually show a cutoff, adsorbing short-chain alkanes but excluding long-chain analogues through selective size-exclusion. Early in 2006, Li et al. developed a Cu-based MOF built on fluorinated organic linker, Cu(hfipbb)(H_2hfipbb)$_{0.5}$ (H_2hfipbb = 4,4′-(hexafluoroisopropylidene)bis(benzoic acid)), which shows clear separation for normal alkanes with a cutoff carbon number of 4 (**Figure 3**).[49] The compound possesses unique 1D channels with alternating large chambers and narrow windows. This type of pore structure is potentially advantageous for size/shape-exclusion-based separation as the narrow windows may act as a splitter to allow the passage of small adsorbates and prohibit inclusion of larger ones. Adsorption experiments revealed that the compound adsorbs noticeable amounts of propane, propylene, and n-butane, but fully excludes normal alkanes with longer chains (e.g., n-pentane, n-hexane, etc.) and branched alkanes (2-methylpropane, 3-methylbutane, etc.). Structural analysis and molecular simulations indicated that the separation is based on size and shape selective molecular exclusion. The chambers, which are wide enough as equilibrium positions, have a length of 7.3 Å, right between the molecular length of n-butane (6.9 Å) and n-pentane (8.1 Å). This explains why the MOF has a fixed carbon number cutoff for the adsorption of normal alkanes. In addition, with a diameter of 3.2 Å, the pore window (neck) is too narrow to be an equilibrium position but allows the passage of normal alkanes while fully excluding branched alkanes. This study serves a perfect example demonstrating the importance of pore shape and pore size of MOFs for the highly efficient separation of alkanes. More recently, the same group reported another MOF, $Zn_2(sdc)_2(bpe)$ (H_2sdc = 4,4′-stilbenedicarboxylic acid, bpe = 1,2-bis(4-pyridyl)ethane), which is capable of separating normal alkanes with a carbon number cutoff at 2.[50] This compound displays a structural

Table 2. Representative MOFs that show size exclusion and highly efficient kinetic-based separations of selected hydrocarbon mixtures and related performance parameters.

Mixtures [units]		MOF[a)]	Pore aperture [Å]	Uptake [wt%][b)]	Selectivity	T [K]/P [kPa]	Experimental methods	Ref.
Normal alkanes	C4/C5+	Cu-hfipbb	3.2	4.0	CME	298/85	GA	[49]
	C2/C3+	$Zn_2(sdc)_2(bpe)$	4.8	2.1	CME	298/100	GA	[50]
	C3/C4+	$Mn(ina)_2$ (F)	4.1	5.9	CME	298/100	GA	[51]
	C4/C5+	Ca(sdb)	5.5	8.2	N.R.	298/25	GA	[52]
Acetylene/ethylene		NbU-1	4.0	7.0	N.R.	298/100	GA/MCB	[59]
		UTSA-100	4.0	11.0	N.R.	298/100	GA/MCB	[57]
		UTSA-200	3.4	13.5	CME	298/100	GA/MCB	[58]
Ethane/ethylene		Ni-gallate	3.5	5.6	CME	298/100	GA/MCB	[73]
		Mg-gallate	3.6	8.7	CME	298/100	GA/MCB	[73]
		Co-gallate	3.7	9.5	CME	298/100	GA/MCB	[73]
		UTSA-280	3.8	11.2	CME	298/100	GA/MCB	[74]
Propane/propylene		ZIF-8	3.4	16	125	303/80	GA	[77]
		$Zn(2\text{-}cim)_2$	3.3	10	160	303/80	GA	[77]
		DTO	5.3	9.2	1.4	298/30	GA	[79]
		TO	5.4	6.3	2.5	298/30	GA	[79]
		DBTO	5.1	4.4	11	298/30	GA	[79]
		BTO	4.7	2.5	12	298/30	GA	[79]
		$Zn(ox)_{0.5}(trz)$ (F)	2.9	10	860	303/85	GA	[80]
				10	1565	323/85	GA	[80]
				7.6	150	363/85	GA	[80]
		$Zn(ox)_{0.5}(atrz)$ (F)	2.6	5	175	303/85	GA	[80]
				5	220	323/85	GA	[80]
		ELM-12	4.0	7	204	298/100	GA/MCB	[81]
				6	971	308/100	GA	[81]
		$Co(aip)(bpy)_{0.5}$	N. R.	8.5	29.7	303/100	GA/MCB	[82]
		MAF-23-O	3.6	5.7	71	298/100	GA/MCB	[84]
		KAUST-7	4.8	5.8	CME	298/100	GA/MCB	[38]
		Y-abtc	4.7	8.2	CME	298/100	GA/MCB	[37]
		Tb-abtc	4.4	9.6	N.R.	298/100	GA/MCB	[83]
C_4 olefins		SD-65 (F)	N.R.	9.6	CME	298/100	GA/MCB	[89]
		GeFSIX-14-Cu-i	4.2	14.8	CME	298/100	GA/MCB	[90]
Alkane isomers	Linear/branched	ZIF-8 (F)	3.4	N.R.	N.R.	N.R.	GC	[97]
	nHEX/3MP, 22DMB	ZIF-8 (F)	3.4	25	N.R.	313/100	VA/MCB	[96]
	nHEX/2MP	ZIF-8 (F)	3.4	50	N.R.	298/N.R.	LA/MCB	[95]
	Linear/branched	ZIF-8 (F)	3.4	N.R.	N.R.	N.R.	MCB	[3]
	nHEX, 2MP, 23DMB/22DMB	ZIF-8 (F)	3.4	22	N.R.	373/80	VA	[94]
	nHEX/3MP, 22DMB	$Zn(bdc)(dabco)_{0.5}$	4.7	6	N.R.	313/35	MCB	[99]
	nHEX/3MP, 23DMB, 22DMB	MIL-127(Fe)	6.0	7.4	N.R.	343/6	MCB	[101]
	nHEX, 3MP/22DMB	Zn(Hbdc)(dmtrz)	7.0	13	N.R.	298/20	VA/GC	[100]
	nHEX, 3MP/22DMB	$Fe_3O(6fdca)_3$	8.0	6	N.R.	298/10	VA/GC	[102]
	nPEN/2MB	Y-fum	4.7	14	CME	293/53	VA/MCB	[103]
	nPEN/2MB	Y-1,4-NDC	5.0	8	N.R.	293/53	VA/MCB	[104]
	nHEX/3MP, 22DMB	Zr-bptc	4.5	13	CME	423/13	VA/MCB	[106]
	nHEX, 3MP/22DMB	Zr-abtc	7.0	11	N.R.	423/13	VA/MCB	[106]
	nHEX, 3MP/22DMB	$Ca(H_2tcpb)$ (F)	5.5	9	CME	333/13	VA/MCB	[108]
	Linear, monobranched/dibranched	Al(bttotb)	5.6	14	CME	303/13	VA/MCB	[109]

Table 2. Continued.

Mixtures [units]		MOF[a)]	Pore aperture [Å]	Uptake [wt%][b)]	Selectivity	T [K]/P [kPa]	Experimental methods	Ref.
C_8 alkylaromatic	*p*X/*o*X/*m*X	Cu(CDC)	5.4	12	N.R.	298/N.R.	LA/MLA	[115]
	*p*X/*o*X/*m*X	CD-MOF-1	9	17	N.R.	318/N.R.	VA/MCB	[118]
	*p*X/*o*X/*m*X	JUC-77	7	7	CME	298/1.0	VA	[119]
	ST/EB/Tol/Bz	MAF-41 (F)	6	24	CME	298/1.0	VA/GC	[110]

[a)]F in parenthesis means flexible MOF; [b)]Showing the uptake of the preferential adsorbate. N.R., not reported; CME, complete molecular-exclusion; GA, gas adsorption; VA, vapor adsorption; LA, liquid adsorption; MCB, multicomponent column breakthrough; MLA, multicomponent liquid adsorption; GC, gas chromatography.

transformation upon solvent exchange and subsequent solvent removal. The activated structure has a small pore size, adsorbing small gases, including CO_2, ethane, ethy—lene, and acetylene, but fully excluding larger molecules such as propane, propylene, and butane. Thus, it acts as an efficient filer for the two groups of normal alkanes. Flexible MOFs have also been found to be capable of separating normal alkanes with different chain lengths as they exhibit very different adsorption behavior toward different normal alkanes. Li and coworkers reported a flexible MOF, $Mn(ina)_2$ (ina = isonicotinate), which shows clear separation of alkanes with a fixed carbon number cutoff of 3, due to its adsorbate-dependent adsorption behavior.[51] The compound exhibits a gate-opening adsorption for CO_2, C_2, and C_3 hydrocarbons with noticeable adsorption capacity. While the structural gate-opening can also be induced by butane at a very low pressure, the adsorbed amount is negligible indicating that the effective pore size upon pore-opening is too small to accommodate butane molecules. The negligible adsorption can be attributed to the adsorption of the alkane chain at the pore mouth, which was also observed in previous studies. Thus, the compound demonstrates selective size-exclusion for normal alkanes with carbon number ≥4.

Adsorption mechanisms of normal alkanes in MOFs have been rarely explored. Among various experimental and computational techniques, determining crystal structures of guest-loaded MOFs would be the most straightforward and powerful one, as it allows the precise identification of the adsorption sites and possible adsorbate–adsorbent interactions. Li et al. investigated the mechanism of adsorption of alkanes in a calcium-based MOF, Ca(sdb) (sdb = sulfonyldibenzoate) (**Figure 4**).[52] Ca(sdb) features a 3D framework with 1D segmented channels, with a diameter of 5.5 Å. Interestingly, it adsorbs moderate amounts of ethane, propane, and butane with fast adsorption kinetics, but its adsorption capacities toward pentane, hexane, and heptane are substantially lower with obvious diffusion restrictions. Single-crystal X-ray diffraction analysis revealed that C_2–C_4 normal alkanes are commensurately adsorbed in the segmented channels of Ca(sdb), with each molecule perfectly accommodated in a channel segment. This is a result of good matching between the pore size/pore shape and the dimen-

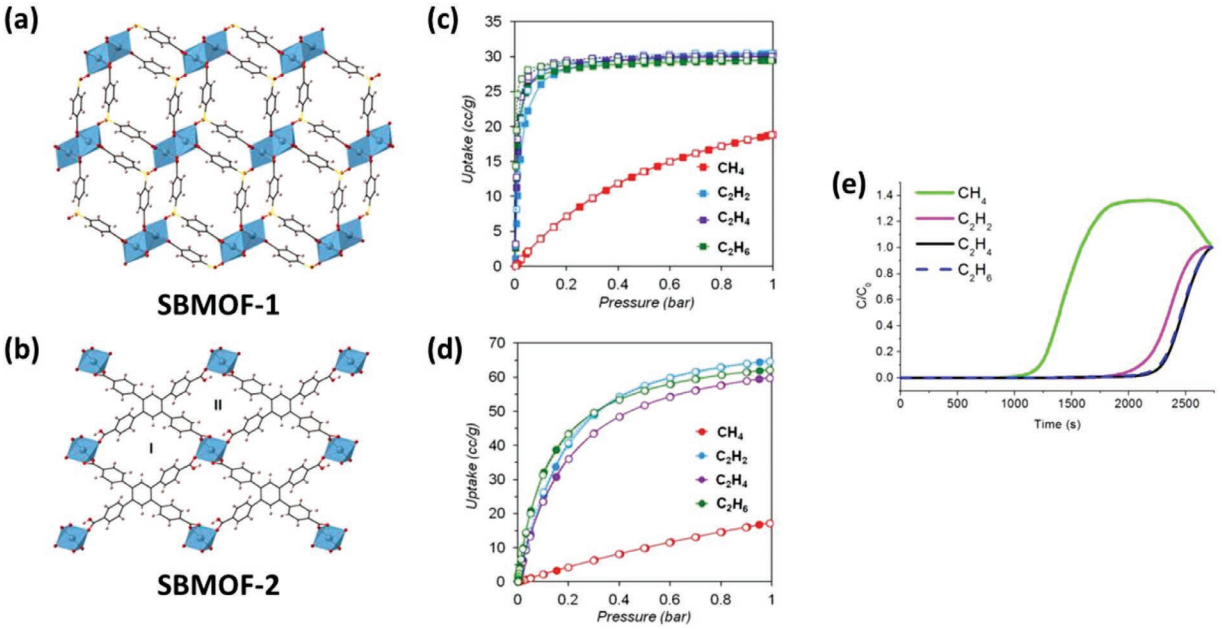

Figure 2. a,b) Crystal structure of SBMOF-1 (a) and SBMOF-2 (b). c,d) Single-component adsorption isotherms of methane and C_2 hydrocarbons at 298 K on SBMOF-1 (c) and SBMOF-2 (d). e) Multicomponent column breakthrough curves for SBMOF-1. Reproduced with permission.[48] Copyright 2016, American Chemical Society.

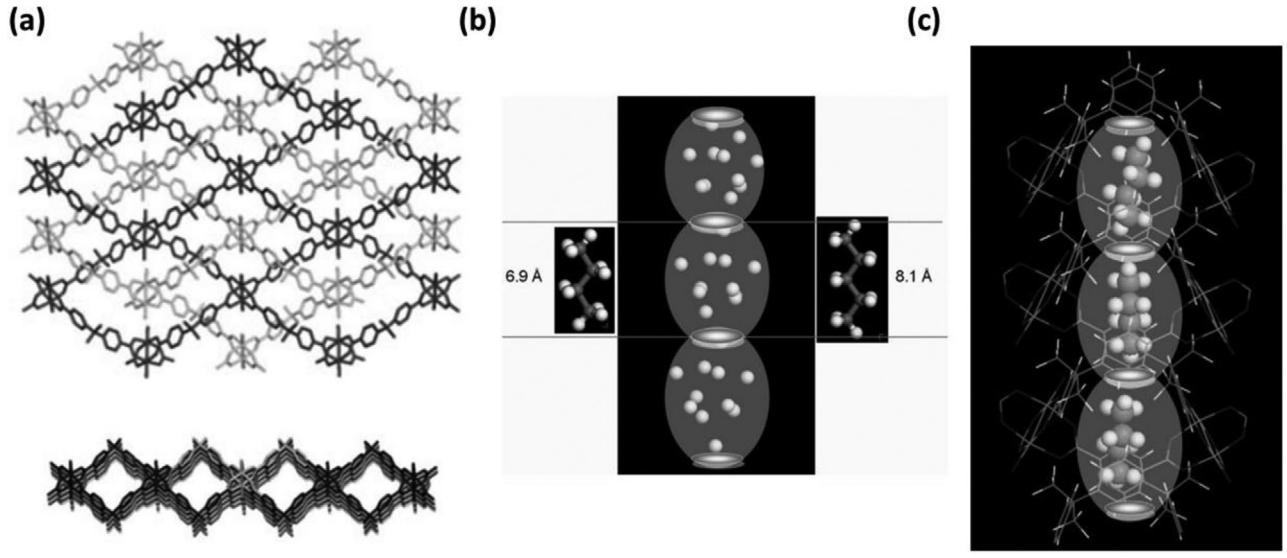

Figure 3. a) Structure view of Cu(hfipbb)(H_2hfipbb)$_{0.5}$ and its 1D tubular micro-channels. b) The shape of the channels in Cu(hfipbb)(H_2hfipbb)$_{0.5}$ outlined by molecular simulation. c) Arrangement of butane molecules in the channel. Reproduced with permission.[49] Copyright 2006, Wiley-VCH.

sions of the adsorbate molecules. In contrast, C_5–C_7 alkanes are disorderly distributed along the channels due to the fact that each molecule cannot fit into each channel segment. The experimental results indicated that the MOF has a carbon number cutoff of 4 toward the adsorption of alkanes with respect to adsorption capacities, kinetics, and accommodation sites. In addition, a transition from commensurate to incommensurate adsorption was observed as carbon number of the normal alkanes increased.

3. Separation of Alkane/Alkene/Alkyne Mixtures

3.1. Acetylene–Ethylene

3.1.1. Background and Representative Examples of Thermodynamic Separation

The purification of ethylene from other C_2 hydrocarbon analogues (including acetylene and ethane) is of great significance

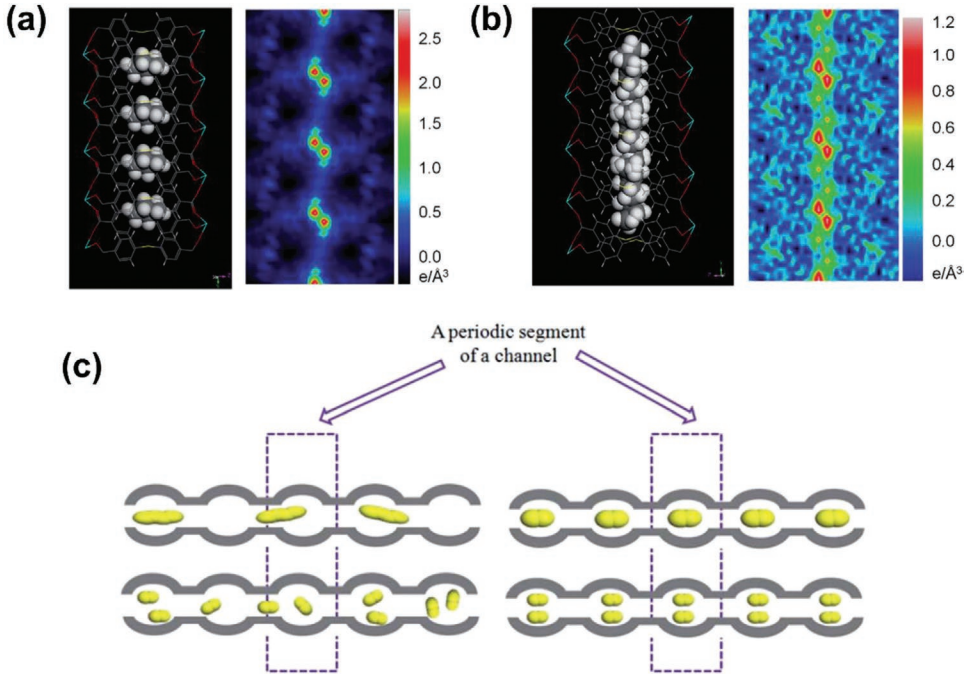

Figure 4. a,b) Packing of alkane molecules and the difference electron density map calculated before assigning the adsorbate for C_3 (a) and C_6 (b) alkanes. c) Pictorial representation of commensurate and incommensurate adsorption with a tubular 1D channel. Reproduced with permission.[52] Copyright 2016, Royal Society of Chemistry.

as polymer-grade ethylene (purity >99.95%) is the starting material for the production of the world's most extensively used synthetic plastic polyethylene. The separation between ethylene and acetylene is particularly important as both components are major feedstock for various industrially important products. Typically, about 1% of acetylene exists in the ethylene stream from thermal cracking reactions, which needs to be removed to produce ethylene with sufficient level of purity. Current technology of removing acetylene from ethylene relies on partial chemical hydrogenation, or solvent extraction. These processes suffer from drawbacks, including over-hydrogenation and environmental destruction. A number of MOFs have demonstrated the capability to separate acetylene and ethylene through thermodynamically driven mechanism.[53,54] MOFs with OMSs could provide specific metal–π interaction and they are capable of differentiating alkynes and alkenes based on the strength of adsorption affinity. The prototype example is the MOF-74 series. MOF-74-M (M = Mg, Mn, Fe, Co, Ni, Zn) contains a high density of OMSs along the 1D channels, leading to preferential adsorption toward acetylene over ethylene. However, the adsorption capacity/affinity of acetylene is only slightly higher than that of ethylene, resulting in limited selectivity. In addition, MOFs with OMSs are generally sensitive to water/moisture and H_2O molecules may also act as a competing adsorbate to hydrocarbons, which may affect the separation efficiency. More recently, Xing et al. reported the pore chemistry and pore size control over the well-known SIFSIX series MOF materials, and highly selective removal of acetylene from ethylene was achieved.[55] SIFSIX MOFs feature pillar-layered structures built on hexafluorosilicate (SiF_6^{2-}) and 4,4-dipyridyl or its derivatives. They possess 1D square-shaped channels decorated with a high density of fluorine atoms, with pore size depending on the geometry and length of the dipyridyl ligands.[56] The authors found that two members of the SIFSIX family, SIFSIX-2-Cu-i and SIFSIX-1-Cu, exhibit exceptional acetylene capture performance from ethylene. Their preferred adsorption of acetylene over ethylene can be attributed to the optimal channel dimensions and geometric disposition of SiF_6^{2-} moieties along the channels, which enable the noticeably preferential binding of acetylene over ethylene. SIFSIX-2-Cu-i adsorbs 2.1 mmol g^{-1} of acetylene at 298 K and 0.025 bar while the adsorbed amount of ethylene is negligible (<0.2 mmol g^{-1}) at such a low pressure. This indicates SIFSIX-2-Cu-i could potentially remove trace acetylene from ethylene. In contrast, while SIFSIX-1-Cu does not adsorb as much acetylene at low pressure, its acetylene adsorption capacity at 298 K and 1 bar is 8.5 mmol g^{-1}, higher than those of MOFs with OMSs including MOF-74-Fe. Its ethylene uptake under identical conditions is substantially lower (≈4 mmol g^{-1}), indicating its potential capability of separating equimolar acetylene/ethylene mixtures. The separation capabilities of these materials were confirmed by experimental column breakthrough studies starting from acetylene/ethylene mixtures with varied compositions. The concentration of acetylene in the ethylene stream eluting from the column was below 2 ppm, yielding ethylene with a purity >99.998%, well meeting the requirement for the production of polyethylene. The excellent capability of SIFSIX MOFs for the removal of acetylene from ethylene is a result of the existence of the so called "sweet spots" in pore chemistry and pore size that enable exceptionally efficient separation that is approaching selective molecular sieving. Similar selective adsorption of acetylene over ethylene based on adsorption strength was also observed on M′MOF-2, M′MOF-3, NOTT-300, and other materials.

3.1.2. Size-Exclusion Based Separation

In light of the difference in molecular dimensions for acetylene and ethylene (kinetic diameter: acetylene 3.3 Å, ethylene 4.2 Å), precise control of MOF pore aperture may be an effective approach to achieve adsorbents with optimal pore structure suitable for size-exclusion-based separation. Chen et al. reported the separation of acetylene and ethylene by a microporous MOF, Cu(ATBDC) (also termed as UTSA-100, H_2ATBDC = 5-(5-amino-1H-tetrazol-1-yl)-1,3-benzenedicarboxylic acid), with suitable pore size and additional amine functional groups (**Figure 5**).[57] The MOF features a 3D structure with 1D channels with a pore diameter of 4.6 Å. The limiting pore aperture of the channel is 3.96 Å, which falls between the kinetic diameters of acetylene and ethylene. Gas adsorption isotherms revealed that acetylene and ethylene could be accommodated by UTSA-100, but the uptake of the latter (1.65 mmol g^{-1} at 296 K and 1 bar) was much lower than that of the former (4.24 mmol g^{-1}) under identical conditions. Multicomponent column breakthrough measurements demonstrated that acetylene was retained in the column for more than 15 min but the retention for ethylene was negligible (<1 min), indicating ethylene was almost fully excluded from the MOF pores under mixed gases conditions. While the amine functional groups in UTSA-100 has contributed to its enhanced adsorption toward acetylene through possible weak acid–base interactions, the optimal pore aperture of the MOF might play a more important role in the sieving effects that lead to its superior adsorption selectivity.

Chen and co-workers developed another microporous MOF, UTSA-200, that can fully separate acetylene from ethylene through size-exclusion mechanism (**Figure 6**).[58] UTSA-200, also known as SIFSIX-14-Cu-i, belongs to the SIFSIX family. The structure is built on SiF_6^{2-} and azpy (4,4′-azopyridine) with 1D channels (diameter: 3.4 Å) that completely block ethylene molecules but allow acetylene to diffuse in. This was attributed to the high tunability of the pore size of SIFSIX materials, which can be finely adjusted by judicious design/selection of the dipyridyl ligands without altering the topology of the framework. Guided by this designing strategy, UTSA-200 was formed by substituting dpa (4,4′-dipyridylacetylene) in the aforementioned SIFSIX-2-Cu-i by azpy, so as to downsize the pore aperture to realize the full exclusion of ethylene. Experimental gas adsorption measurements showed that UTSA-200 adsorbs 116 and 58 cm^3 cm^{-3} of acetylene at 1 and 0.01 bar, respectively, at 298 K. The volumetric uptakes of UTSA-200 are higher than those of SIFSIX-2-Cu-i, although the pore volume of the former is smaller due to the utilization of a shorter organic ligand. These findings indicate that the contraction of the pore size in UTSA-200 is the main reason for enhanced adsorption affinity toward acetylene and improved packing efficiency. In contrast, UTSA-200 adsorbs very little ethylene under identical conditions, with ≈15 cm^3 cm^{-3} at 1 bar and negligible amount at 0.01 bar. Experimental multicomponent column breakthrough studies for acetylene/ethylene (1:99, v/v) mixture revealed that

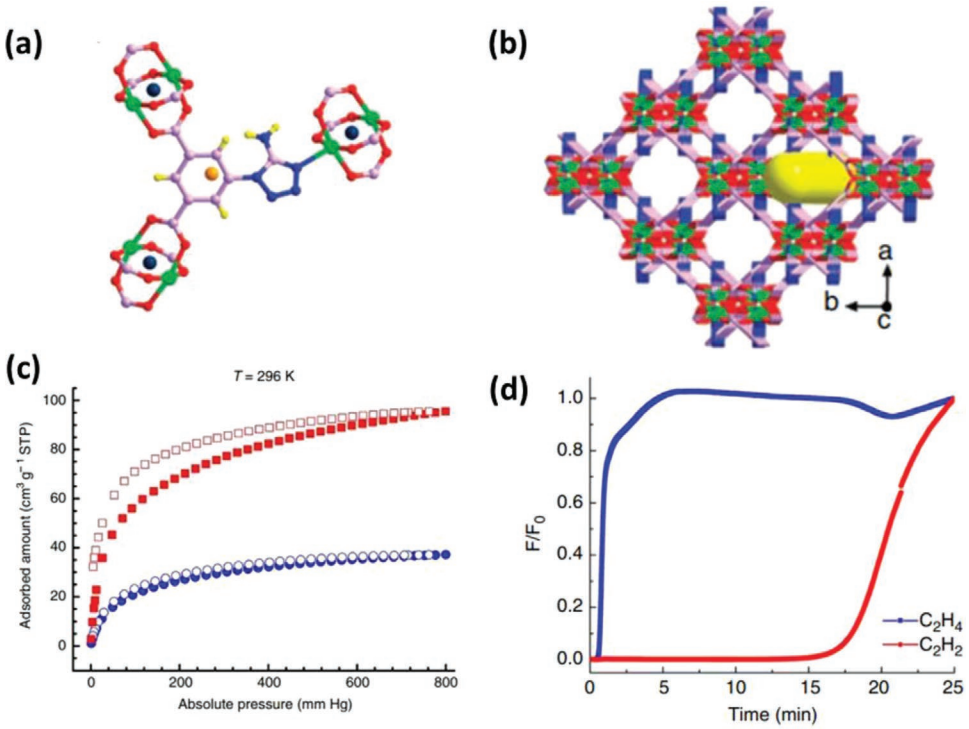

Figure 5. a,b) The coordination environment (a) and 3D structure (b) of UTSA-100. c) Acetylene and ethylene sorption isotherms at 296 K. d) Experimental column breakthrough curve for acetylene/ethylene mixed gas containing 1% acetylene over UTSA-100 at 296 K. Reproduced with permission. Copyright 2015,[57] Springer Nature.

ethylene eluted out immediately while acetylene was retained in the column for a substantially long time. The eluted ethylene stream had a purity of 99.9999% with less than 1 ppm of acetylene. The acetylene level was noticeably lower than the maximum allowed concentration (40 ppm) for the production of polyethylene. Further exploration of adsorption mechanisms through determining the crystal structure of acetylene-loaded UTSA-200 confirmed that its preferential adsorption toward acetylene was a result of its optimal pore chemistry and pore size and their perfect matching with acetylene molecules. This study demonstrates the important role of reticular chemistry in fine tuning MOF pore size to achieve optimum separations.

Another MOF material exhibiting highly efficient kinetic separation of acetylene and ethylene was recently reported by Li et al., with a formula of $(NH_4)\{Cu^{II}_3\cdot[Cu^{II}Cu^{I}_6(OH)_6(Ad)_6]_2\}$ (also termed as NbU-1, Ad = adenine).[59] The MOF was built on mixed-valence heptanuclear $Cu_7(OH)_6$ clusters and single Cu ions linked by adenine ligands. The 3D structure of NbU-1 possesses 1D channels with a pore size of ≈4 Å. Gas adsorption measurements revealed that NbU-1 adsorbs markedly higher acetylene (≈3.79 mmol g^{-1}) than that of ethylene (≈2.14 mmol g^{-1}) under identical conditions (273 K and 1 bar). However, the calculated heat of adsorption for the two gases (38.3 and 37.9 kJ mol^{-1} for acetylene and ethylene, respectively) are very similar, indicating that difference in adsorption affinity was not the reason for the uptake difference. Further analysis showed that NbU-1 underwent noticeably different adsorption kinetics for acetylene and ethylene, with a substantially higher adsorption rate for the former than that of the latter, suggesting it was a kinetically driven separation originating from the suitable pore aperture of the MOF. Multicomponent column breakthrough experiments of a mixture of acetylene/ethylene (1/99, v/v) confirmed that the material was capable of removing trace acetylene from ethylene and producing ethylene with a purity >99.997%.

3.2. Ethylene–Ethane

3.2.1. Background and Representative Examples of Thermodynamic Separation

As stated in the previous section, ethylene is the most important olefin in industry because it is the feedstock for the production of polyethylene, the world's most widely used synthetic plastic. The annual global demand for ethylene exceeds 150 million metric tons and such demand will continue to rise. Besides acetylene/ethylene separation, the purification of ethylene also involves the removal of ethane. Traditional separation of ethylene and ethane relies on heat-driven fractional distillations, which involve repeated distillation–compression cycling of the mixture under cryogenic temperature in a huge separating column with more than 100 trays.[4] This process consumes about 7.3 GJ energy per ton of ethylene, which could be potentially reduced if non-thermal separation technologies (e.g., adsorption/membrane-based separation) are employed. The exploration of an ideal adsorbent with high ethylene/ethane separation performance is critical for the implementation of non-thermal separation processes.

MOFs with OMSs have been extensively investigated for the thermodynamic separation of ethane and ethylene, and they

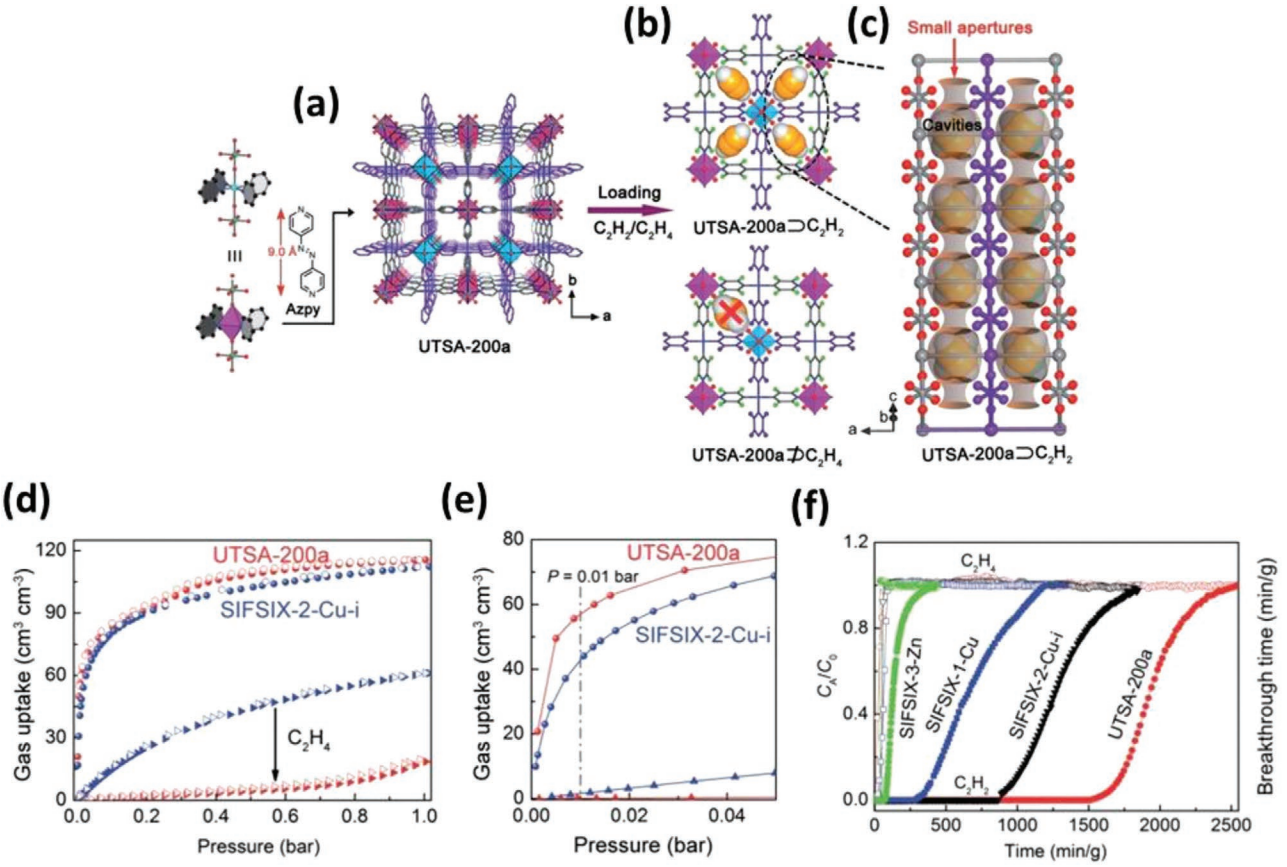

Figure 6. a) Crystal structure of UTSA-200 showing its 1D channels. b) DFT-D-calculated acetylene adsorption models in UTSA-200, revealing that its pore size allows the passage of acetylene molecules and the simulated ethylene adsorption in UTSA-200 indicating that ethylene molecules are too large to pass through the pores. c) Schematic illustration of ideal molecular sieves based on the structure of UTSA-200, in which larger cavities suitable for strongly binding acetylene molecules are interconnected by narrow apertures that serve as sieves for ethylene but not for acetylene. d,e) Acetylene and ethylene adsorption isotherms on UTSA-200 in the pressure range of 0–1.0 bar (d) and 0–0.05 bar (e). f) Experimental column breakthrough curves for acetylene/ethylene separations with UTSA-200 and related materials under identical conditions at 298 K and 1.01 bar. Reproduced with permission.[58] Copyright 2017, Wiley-VCH.

are expected to show higher efficiency toward ethane/ethylene separation compared to acetylene/ethylene separation. This is because different from acetylene and ethylene ethane lacks unsaturated bonds that would interact specifically with OMSs, resulting in relatively large difference in adsorption affinity for ethane and ethylene with MOFs containing OMSs. MOF-74-M (M = Mg, Mn, Fe, Co, Ni, Zn) series serves as a representative example of this type of materials. MOF-74-M features 1D channels decorated with a high density of OMSs, which selectively interact with olefins with higher adsorption affinity than that of their corresponding paraffins, with a olefin/paraffin IAST selectivity of 3–15.[34,47] This thermodynamically controlled separation applies to ethylene/ethane, propylene/propane, and other olefin/paraffin mixtures.

Ethylene-selective materials are common among known adsorbents. However, in rare cases reversed ethane-selective behavior has been observed, such as in some zeolites.[60] Recently, the same behavior has also been discovered in a group of MOFs.[38,61–69] This phenomenon is contrary to most MOFs which usually demonstrate preferential adsorption toward ethylene over ethane due to the specific interaction between the carbon–carbon double bond and the immobilized metal centers. Ethane-selective MOFs could be of great use as their removal of trace ethane from ethylene (rather than the reverse process) is much more energy and cost effective. Li et al. reported the selective adsorption of ethane over ethylene by a MOF with iron-peroxo sites, Fe_2O_2(dobdc).[69] Fe_2O_2(dobdc) was obtained by oxidizing MOF-74-Fe, an extensively investigated MOF structure with a high density of OMSs. Single-component adsorption isotherm revealed reversible adsorption of ethylene and ethane by Fe_2O_2(dobdc), with noticeably higher adsorption capacity for ethane over ethylene. This is different from the pristine compound MOF-74-Fe which took up more ethylene than ethane because of the open Fe(II) sites. The calculated ethane/ethylene IAST adsorption selectivity for Fe_2O_2(dobdc) was 4.4, a value that is higher than those of all other ethane-selective adsorbents, including MOFs and zeolites. Multicomponent column breakthrough measurements starting from ethane/ethylene mixtures with different compositions confirmed the separation capability of the material. Ethane was retained in the column for a substantially longer time than that of ethylene, yielding ethylene with a purity of 99.95%

which meets the requirement for the production of polyethylene. High-resolution neutron powder diffraction analysis and first-principles dispersion-corrected density functional theory calculations revealed that the high ethane/ethylene selectivity originated from the hydrogen bonds between ethane and the peroxo sites. In addition, the authors found ethane molecules match better with the channel size of Fe_2O_2(dobdc) than ethylene, leading to sufficient contacts and stronger van der Waals interactions. However, it is noteworthy that the material is air sensitive and needs to be handled and stored in a dry box under inert atmosphere. Prior to this work, Zhang et al. reported the selective trapping of ethane from ethylene by a porous metal–azolate framework Zn(batz) (MAF-49, H_2batz = Bis(5-amino-1H-1,2,4-triazol-3-yl)methane).[70] This compound adsorbs similar amounts of ethane and ethylene under equilibrium conditions at 1 bar. However, It was observed that ethane was preferentially adsorbed at low pressure region, and the heat of adsorption for ethane (≈60 kJ mol^{-1}) was noticeably higher than that for ethylene (≈48 kJ mol^{-1}). Monte Carlo simulations and density functional theory optimization of guest-loaded structure revealed that ethane forms strong hydrogen bonds with the organic linker of the MOF, while for ethylene the interactions are relatively weaker. Multicomponent column breakthrough experiments mimicking industrial mixtures comprising ethane, ethylene, methane, and carbon dioxide confirmed that ethane was retained in the column for the longest time and polymer-grade ethylene (purity >99.95%) could be obtained with relatively high efficiency. Other ethane-selective MOFs include PCN-250,[66] PCN-245,[65] ZIF-7,[71–72] MIL-142,[64] and recently reported $Cu(Qc)_2$[67] and MUF-15.[61]

3.2.2. Size-Exclusion-Based Separation

The aforementioned ethane-selective MOF adsorbents could be beneficial under circumstances where trace ethane needs to be removed from ethylene. However, with relatively low adsorption selectivities, the general performance level of these ethane-selective adsorbents is inefficient for the commercial separation process, particularly when ethane takes up a large proportion of the ethylene stream. Over the past few years, research efforts have been made continuously to develop ethylene-selective MOFs with high adsorption selectivities, especially those capable of kinetic separation or selective size/shape-exclusion based separation. Bao et al. reported a series of gallate-based MOFs that show selective molecular-sieving of ethane from ethylene (**Figure 7**).[73] M-gallate (M = Ni, Mg, Co) structure possesses 3D interconnected zigzag channels with aperture size in the range of 3.47–3.69 Å (3.47, 3.56, and 3.69 Å for the Ni, Mg, and Co-gallate, respectively), noticeably smaller than the kinetic diameter of ethylene or ethane. Thus, one may expect it would exclude both gases based on the values of their kinetic diameters. However, the aperture size is slightly larger than the minimum cross-section size of ethylene molecule (3.28 × 4.18 Å), but smaller than that of ethane (3.81 × 4.08 Å). This indicates that the material might be able to separate the two gases through molecular cross-section size differentiation, which was confirmed by experimental results. Taking Co-gallate as an example, it adsorbed 3.37 mmol g^{-1} of ethylene at 298 K and 1 bar, but substantially less ethane (≈0.3 mmol g^{-1}) under identical conditions, with an IAST selectivity of 52. The exceptionally high selectivity set a new record for the separation of

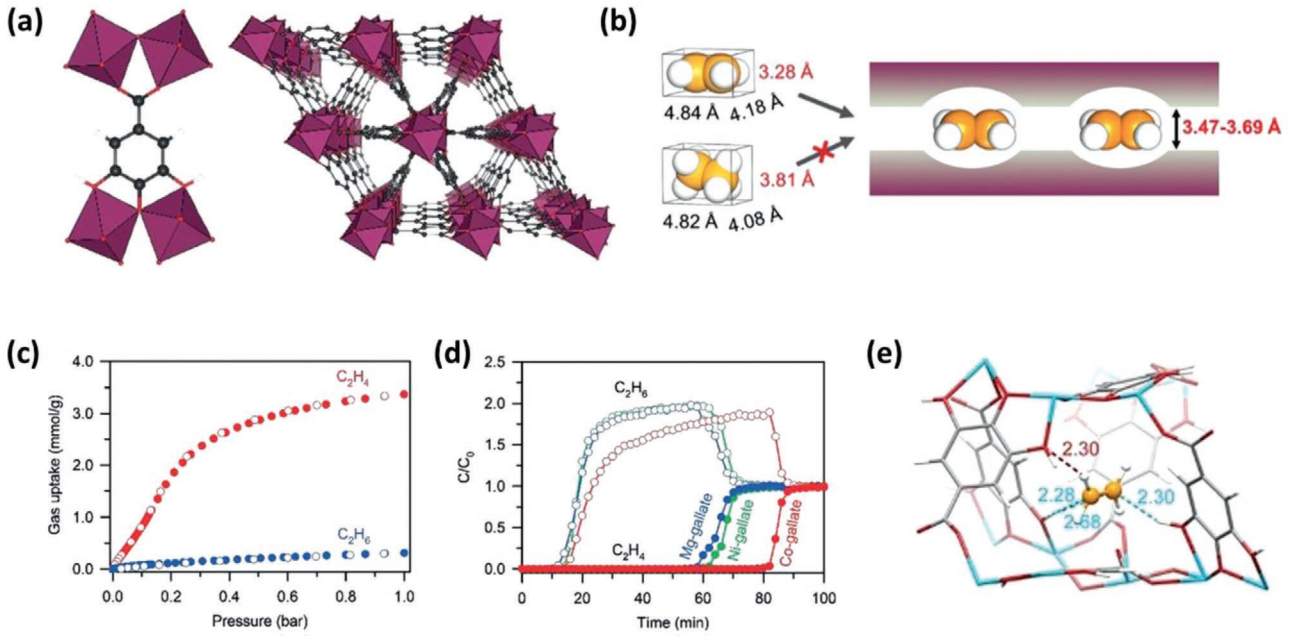

Figure 7. a) Coordination environment and perspective view of the crystal structure of M-gallate. b) Diagram of the fusiform branched channels. Only ethylene can favorably enter the cavity because the limiting aperture size of M-gallate matches well with the smallest cross-section size of ethylene (3.28 × 4.18 $Å^2$), but it is smaller than that of ethane (3.81 × 4.08 $Å^2$). c) Single-component adsorption isotherms of ethylene and ethane in Co-gallate at 298 K in the pressure range of 0–1 bar. d) Experimental breakthrough curves of M-gallate for the equimolar ethylene/ethane mixture at 273 K and 1 bar with a constant flow rate of 0.5 mL min^{-1}. e) Primary adsorption site of ethylene in Mg-gallate, identified through neutron diffraction. Reproduced with permission.[73] Copyright 2018, Wiley-VCH.

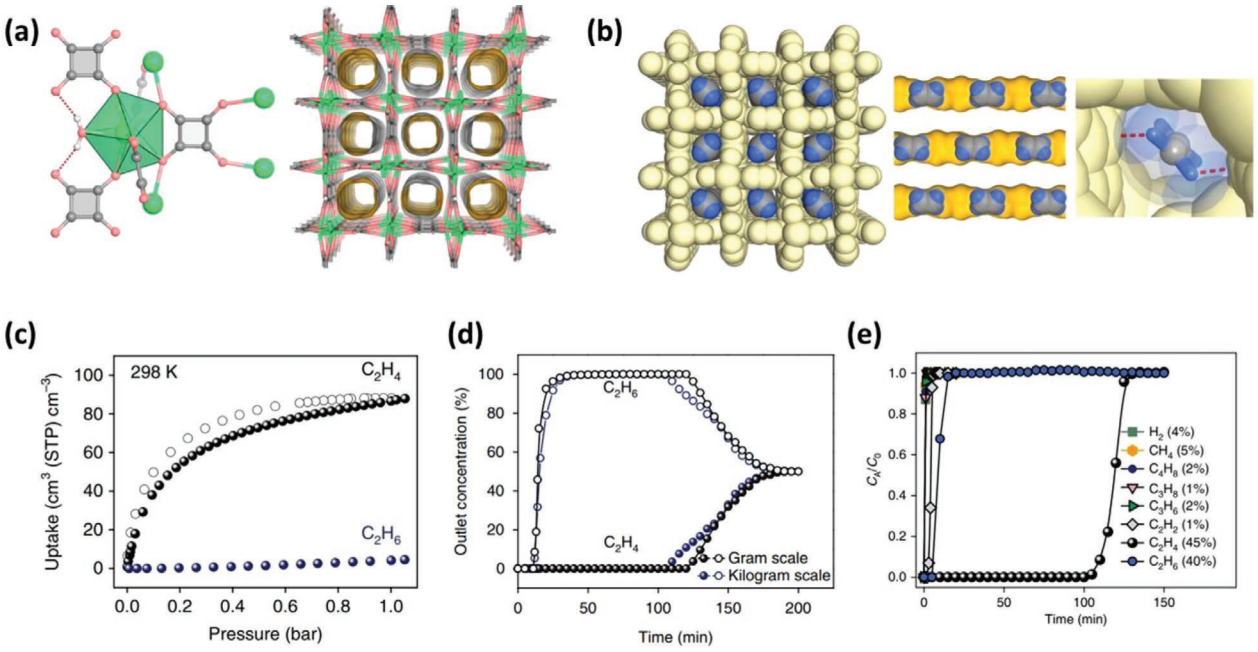

Figure 8. a) Local coordination environments and perspective view of crystal structure of UTSA-280. b) Packing diagram and preferential binding site for adsorbed ethylene in UTSA-280, determined through single-crystal X-ray diffraction study. c) Single-component sorption isotherms of ethylene and ethane at 298 K for UTSA-280. d) Breakthrough curves for UTSA-280 from different scales for an equimolar binary mixture of ethylene/ethane at 298 K and 1 bar. e) Multi-component breakthrough curves for an octonary mixture at 298 K and 1 bar. Reproduced with permission.[74] Copyright 2018, Springer Nature.

ethane and ethylene. On the other hand, the fact that M-gallate adsorbed negligible amount of ethane implies that the molecule was excluded from entering the channels. Column breakthrough tests for an equimolar mixture of ethane and ethylene confirmed that ethane was barely retained in the column and the material was capable of well separating the two gases. The adsorption sites of ethylene in M-gallate was further explored by high-resolution neutron powder diffraction measurements, and the results revealed high utilization efficiency of the quasi-discrete branched channels and existence of cooperative supramolecular interactions for the adsorption of ethylene. This study clearly suggests that while kinetic diameter is an important parameter to consider when designing adsorbents for the separation of similar molecules, the minimum cross-section cannot be neglected, especially for those with their molecular shapes largely deviated from a sphere.

Among all previously discussed examples, including MOFs with OMSs and those showing ethane-selective separation, while one adsorbate is preferentially adsorbed, sometimes with high adsorption selectivity, the co-adsorption of the other adsorbate is inevitable. In the case of M-gallate, though the separation is close to size exclusion, moderate adsorption of ethane was also detected, indicating that ethane is not completely excluded by the adsorbent. Complete molecular sieving that avoids the co-adsorption of impurities and offers infinite adsorption selectivity, is ideal for maximizing the separation efficiency, and would also be beneficial for membrane-based separations. However, separation based on complete size exclusion of molecules with similar size/shape is challenging and requires a precise match between the adsorbates and the MOF pore structure to gain a specific recognition of selected adsorbates. Recently, Chen et al. reported complete ethane-exclusion from ethylene by a rigid MOF (**Figure 8**).[74] The compound, $Ca(C_4O_4)(H_2O)$ (UTSA-280, $H_2C_4O_4$ = squaric acid), which was first reported in 1987, represents a 3D framework with 1D open cylindrical channels. The cross-sectional area of the 1D channels is 14.4 $Å^2$, which falls between the minimum cross-sectional areas of ethylene (13.7 $Å^2$) and ethane (15.5 $Å^2$), indicating that UTSA-280 may serve as a splitter capable of complete separation of the two gases. The hypothesis was validated by experimental results. The compound adsorbed 2.5 mmol g^{-1} of ethylene at 298 K and 1 bar, and in contrast, its uptake for ethane was essentially negligible (<0.1 mmol g^{-1}) under identical conditions. This result suggests that ethane was fully excluded by the 1D channels, consistent with the fact that the cross-sectional area of the channels is smaller than that of ethane. The adsorption capacity toward ethylene was higher than those of extensively studied zeolites, including zeolite 5A and cation-exchange ETS-10. The ethylene adsorbed in the channels reached a density of 389 g L^{-1}, close to the density of liquid ethylene (568 g L^{-1}). The high packing density of ethylene inside the channels of UTSA-280 was attributed to the perfect matching between the size/shape of the adsorbate molecule and the channel dimensions, which was experimentally confirmed by single-crystal X-ray diffraction studies and theoretical computations. Crystal structure of ethylene-loaded UTSA-280 reveals that ethylene molecules adopt optimal orientation, with its minimum cross-section along the diagonal of the pore aperture so as to minimize any possible steric hindrance and electrostatic repulsion from the framework. In contrast, significant steric hindrance will be unavoidable when ethane molecules are put inside the channels with whichever orientations, in good agreement with

the noticeably higher potential energy variations for ethane along the channels from DFT calculations. Based on the results of column breakthrough experiments of an equimolar ethane/ethylene mixture, ethane showed almost no retention while ethylene was retained in the column for a substantially longer time, yielding a dynamic ethylene capacity of 1.86 mol kg^{-1}. The adsorbed ethylene can be removed easily under He flow at 353 K. In addition, multicomponent breakthrough experiments were carried out on an octonary $H_2/CH_4/C_2H_2/C_2H_4/C_2H_6/C_3H_6/C_3H_8/C_4H_8$ mixture (4/5/1/45/40/2/1/2), mimicking the real steam from ethane cracking reactions. The results show that the MOF was competent to exclusively enrich ethylene from the complicated mixture, indicating that the gas impurities would not affect the separation capability of the material. Importantly, UTSA-280 could be easily scaled up and showed excellent stability toward water/moisture and good recyclability, making it promising for industrial implementation.

3.3. Propylene–Propane

3.3.1. Background and Representative Examples of Thermodynamic Separation

Propylene is the starting material for the production of polypropylene, the world's second-most widely produced synthetic plastic. Propylene is produced mainly from two processes in petrochemical industry, steam cracking of naphtha and catalytic cracking of gas oils. In both cases, propane coexists with propylene as binary mixtures, with a propylene purity of 50–60% for the former and 80–87% for the latter. Propane needs to be removed from the mixture so as to yield polymer-grade propylene with a purity ≥99.5%, to meet the requirement for the production of polypropylene.[38] Currently applied separation process of propane and propylene by cryogenic separation is carried out at about 243 K and 0.3 MPa in a column containing over 100 trays, which is of high energy penalty. The United States Department of Energy has identified the separation of propane and propylene as the most energy-intensive single distillation process employed in industry. Several zeolite materials, including zeolite 4A, zeolite 5A, and chabazite (CHA) have been widely explored for adsorptive separation of propane and propylene.[2] Zeolite 4A adsorbs propylene only and fully excludes propane, thus serving as an example of selective size-exclusion-based separation. However, the adsorption kinetics of propylene on zeolite 4A is noticeably slow, resulting in relatively poor propane/propylene separation under ambient conditions. Chabazite zeolite shows obvious diffusional restrictions for propane but adsorbs propylene freely, exhibiting kinetic separation. Nevertheless, a comparative study of zeolite 4A and chabazite zeolite for separation of propane and propylene at the process level indicates that the performance of chabazite is even lower than that of zeolite 4A, with lower kinetic selectivity and higher energy input.[2]

Generally, MOFs with OMSs are capable of separating propane and propylene based on differences in adsorption affinities, in a similar fashion to the thermodynamic separation of ethane and ethylene, or other olefin/paraffin mixtures. Representative examples include HKUST-1, MOF-74 series, and NOTT-300.[47,75,76] Considering the molecular size difference of propane and propylene, separation by size-differentiation is also possible and has been well demonstrated.

3.3.2. Kinetic Separation

The first example of using MOFs for highly efficient kinetic separation of propane and propylene was reported by Li and coworkers.[77] The authors explored the equilibrium adsorption isotherms and adsorption rates of propane and propylene on a series of ZIF materials, including $Zn(2\text{-mim})_2$ (ZIF-8, 2-mim = 2-methylimidazole) and $Zn(2\text{-cim})_2$ (2-cim = 2-chloroimidazole). While these materials exhibit essentially identical adsorption capacities for propane and propylene under equilibrium conditions, they show markedly different adsorption kinetics for the two gases. The ratios of diffusion rate coefficients for propylene/propane were calculated to be 125 and 60 for $Zn(2\text{-mim})_2$ and $Zn(2\text{-cim})_2$, respectively. This indicates that these materials have the potential to separate propane and propylene based on a kinetically controlled mechanism. More recently, Maurin et al. explored the mechanical control of kinetic separation of propane and propylene by ZIF-8.[78] The stimulus-induced structural flexibility of ZIF-8 allowed the authors to observe evolution of adsorption behaviors under different external pressures. An order of magnitude increase of kinetic selectivity was achieved when 1 Gpa pressure was applied compared to that under ambient condition. This may be attributed to the mechanical control of the gate size and the ligand flip/libration modes of the imidazole linker upon adsorption, under the stimulus of external pressure. Nguyen et al. investigated the separation of propane and propylene by a series of isostructural zinc-pillared-paddlewheel MOF structures (**Figure 9**).[79] Through ligand functionalization, the authors were able to finely tune the pore aperture of this series of MOFs while keeping their framework connectivity unaltered. The pore apertures of this series of four MOF structures, named as DTO, TO, DBTO, and BTO, were successfully tuned from 5.39 to 5.27, 5.10, and 4.67 Å, and the corresponding BET surface areas are 669, 512, 457, and 283 $m^2\ g^{-1}$, respectively. While DTO and TO showed essentially identical equilibrium adsorption capacities and adsorption rates for propane and propylene, DBTO and BTO exhibited noticeably different adsorption kinetics for propane and propylene, with kinetic selectivities of 11 and 12, respectively. This early study serves as an excellent example of the fine-tuning of MOF pore aperture through topology-directed ligand design/functionalization for the kinetic separation of propane and propylene. More recently, highly efficient kinetic separation of propane and propylene was achieved by two isoreticular MOF structures, $Zn(ox)_{0.5}(trz)$ (ox = oxalate, trz = 1,2,4-triazole) and $Zn(ox)_{0.5}(atrz)$ (atrz = 3-amino-1,2,4-triazole).[80] They possess 1D zigzag channels consisting of segments connected through narrow necks (≈3 Å). The adsorption isotherms of propane and propylene were collected at temperatures from 303 to 363 K. Both compounds showed relatively fast adsorption for propylene but marked diffusion restrictions for propane. The kinetic selectivities are 860 and 175 for $Zn(ox)_{0.5}(trz)$ and $Zn(ox)_{0.5}(atrz)$, respectively. These values are noticeably higher than those previously reported for ZIF-8 series and DBTO/BTO, which should

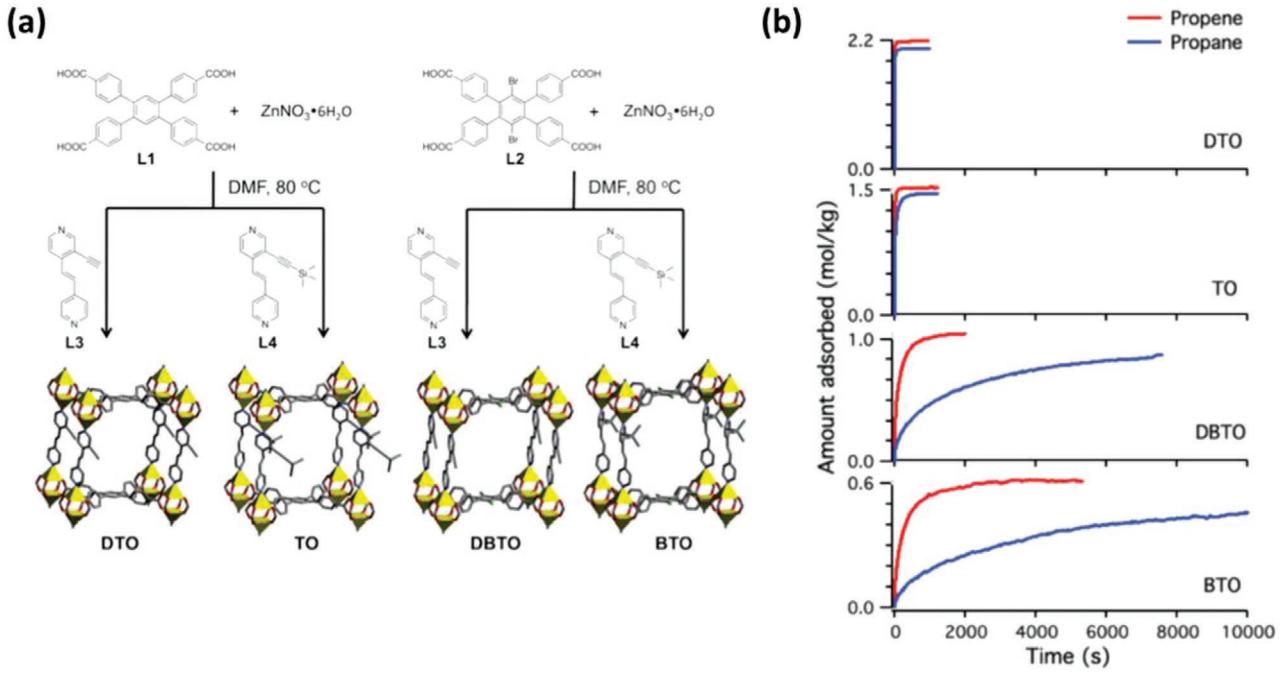

Figure 9. a) Synthesis and crystal structures of the isostructural MOFs DTO, TO, DBTO, and BTO. b) Time-dependent adsorption of propane and propylene by DTO, TO, DBTO, and BTO at 0.3 bar and 298 K. Reproduced with permission.[79] Copyright 2011, American Chemical Society.

be attributed to the optimum pore structure (pore aperture and pore shape) for these two compounds.

Chen et al. reported the development of a microporous MOF, $Cu(bipy)_2(Otf)_2$ (ELM-12, bipy = 4,4′-bipyridine, Otf = trifluoromethanesulfonate), for kinetic separation of propane and propylene with high selectivity.[81] The structure possesses 2D zigzag channels with pore window of 4.0 Å. Time-dependent kinetic adsorption of propane and propylene at 298 and 308 K shows that the compound underwent considerably faster adsorption toward propylene over propane, yielding kinetic selectivities of 204 and 971 at 298 and 308 K, respectively. The propylene/propane kinetic selectivity of ELM-12 surpasses that of the above-mentioned materials under similar conditions, as a result of its optimal pore size and pore shape. Column breakthrough experiments confirmed the separation capability of ELM-12, and after five adsorption–desorption cycles, its separation performance was well-maintained. Importantly, scale-up synthesis of ELM-12 in kilogram quantity was carried out to produce samples with identical structure completeness and separation capability as that from small-scale synthesis. These results confirmed robustness and high processability of ELM-12, which is of great importance for industrial implementation yet often neglected. Very recently, Xia et al. reported the separation of propane and propylene on a cobalt-based pillar-layer MOF, $Co(aip)(bpy)_{0.5}$ (aip = 5-aip aminoisophthalic acid, bpy = 4,4′-bipyridine), with 1D channel of ≈4.5 Å in diameter.[82] Equilibrium adsorption isotherms displayed that it adsorbed 8.5 wt% of propylene but substantially less propane (≈2 wt%) which is close to a case of selective size exclusion. Exploration of its adsorption kinetics confirmed that the adsorption rate for propylene was much faster than that of propane, with a kinetic selectivity of ≈30. Multicomponent column breakthrough experiments confirmed that the material can efficiently separate propane and propylene, with no loss of separation capability after five adsorption–desorption cycles. In addition, the material features high framework stability toward water and moisture. Its adsorption capacity was well-retained after exposure to high humidity or liquid water.

3.3.3. Size-Exclusion-Based Separation

A representative MOF for size-exclusion-based separation of propane and propylene is KAUST-7 (also known as NbOFFIVE-1-Ni), developed by Eddaoudi and co-workers. The study represents an excellent example of reticular chemistry approach (**Figure 10**).[38] The structure of KAUST-7 is a microporous 3D framework built on Ni(II)-pyrazine square-grid layers pillared by $(NbOF_5)^{2-}$ struts. It possesses square-shaped channels decorated by a periodic array of fluoride anions. Structurally, it could be regarded as a derivative compound of the aforementioned SIFSIX series. The previously reported SIFSIX-3-Ni exhibits impressive property of direct CO_2 capture from air; however, it adsorbs both propane and propylene due to its relatively large pore apertures (5.0–7.3 Å). To downsize the pore aperture suitable for effective separation of propane and propylene, the inorganic pillar $(SiF_6)^{2-}$ was substituted by a new pillar $(NbOF_5)^{2-}$ with a larger cation. This strategy was proven successful. The primitive cubic topology was retained in the resultant structure, with reduced pore aperture of 3.0 to 4.8 Å, depending on the steric hindrance between pyrazine molecules and the $(SiF_6)^{2-}$ pillars as a result of the rotation of the pillar. The pore aperture proved to be optimum for the discrimination of propane and propylene. Based on the single component gas

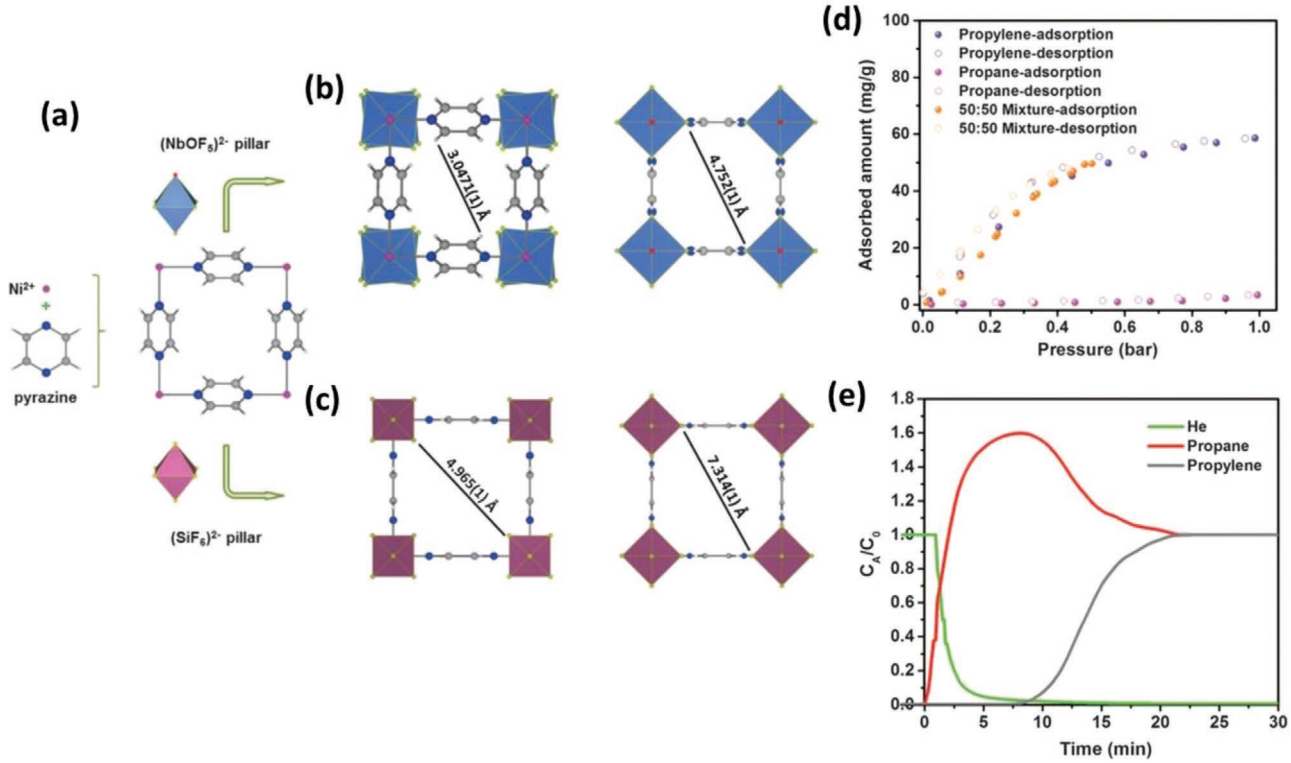

Figure 10. a) Illustration of the square-shaped arrangement in the Ni-pyrazine (4,4′) square grid that is further pillared by inorganic blocks [$(NbOF_5)^{2-}$ or $(SiF_6)^{2-}$] to generate 3D MOFs with a primitive cubic topology. b) Crystal structure and simulation of the maximum open framework of KAUST-7. c) Crystal structure and simulation of the maximum open framework of SIFSIX-3-Ni. d) Single component and an equimolar binary mixture of propane and propylene adsorption isotherms at 298 K up to 1 bar. e) Column breakthrough curves for an equimolar binary mixture at 298 K. Reproduced with permission.[38] Copyright 2016, AAAS.

adsorption data, the material adsorbs ≈6 wt% of propylene at 298 K and 1 bar, but shows essentially no propane uptake under the same conditions. Its selective size-exclusion behavior was confirmed by simultaneous calorimetric and gravimetric measurements, from which the heat of adsorption for propylene was estimated to be 57.4 kJ mol^{-1} while no detectable heat change was observed for propane. The separation capability was further confirmed by mixed-gas column breakthrough experiments, where propylene exhibited a substantial retention while propane was not adsorbed in the column, suggesting a size-exclusion-based separation. Importantly, the authors evaluated the processability of using KAUST-7 for the separation of propane and propylene by a concentration swing recycling mode (CSRM) over multiple adsorption–desorption cycles. The results indicated that KAUST-7 had a propylene uptake/recovery of ≈2 mol kg^{-1} per hour, starting from a propane/propylene 50/50 mixture. In addition, its adsorption capacity and selective size-exclusion behavior were fully maintained after ten adsorption/desorption cycles. The evaluation of zeolite 4A and 5A under identical conditions suggested that they suffer either low adsorption capacity/separation efficiency or material stability.

Early practices of reticular chemistry for tuning MOF pore structure/functionality were focused mainly on the design/functionalization of organic linkers. Recent studies have demonstrated that the rational design of inorganic SBUs can be equally effective. By a combined strategy of ligand design and SBU replacement, a tailor-made MOF, $Y_6(OH)_8(abtc)_3(H_2O)_6(DMA)_2$ (Y-abtc, abtc = 3,3′,5,5′-azobenzene-tetracarboxylates; DMA = dimethylammonium), has been developed for full separation of propane and propylene (**Figure 11**).[37] The authors investigated four MOFs based on the combinations of two SBUs (Zr_6 and Y_6) and two organic ligands (bptc = 3,3′,5,5′-biphenyltetracarboxylates and abtc). Zr_6 and Y_6 are both hexanuclear SBUs with identical mode of propagation by organic linkers, with the highest possible connectivity of 12. The difference is, while Zr_6-based MOFs feature neutral structures, frameworks built on Y_6 are anionic with balancing cations residing inside the pores. Bptc and abtc are rectangular-shaped linkers with different aspect ratios which could affect the topology of the resulting MOFs. Interestingly, Zr-bptc features 12-c ftw topology but Zr-abtc adopts an 8-c scu structure type, indicating that the increase of aspect ratio leads to the decrease of connectivity and transformation of pore structure from cages to 1D open channels. In contrast, both Y-bptc and Y-abtc have the ftw topology, suggesting that Y_6 SBU has a higher tolerance for the aspect ratios of organic ligands. Adsorption experiments show that the pore apertures of Zr-bptc and Zr-abtc are sufficiently large to adsorb both propane and propylene without noticeable diffusional restrictions or differences in adsorption affinity. By contrast, the pore aperture of Y-bptc is too small to adsorb either of the two gases. With the same ligand and identical topology, the significant difference in the pore size of Zr-bptc and Y-bptc should be attributed

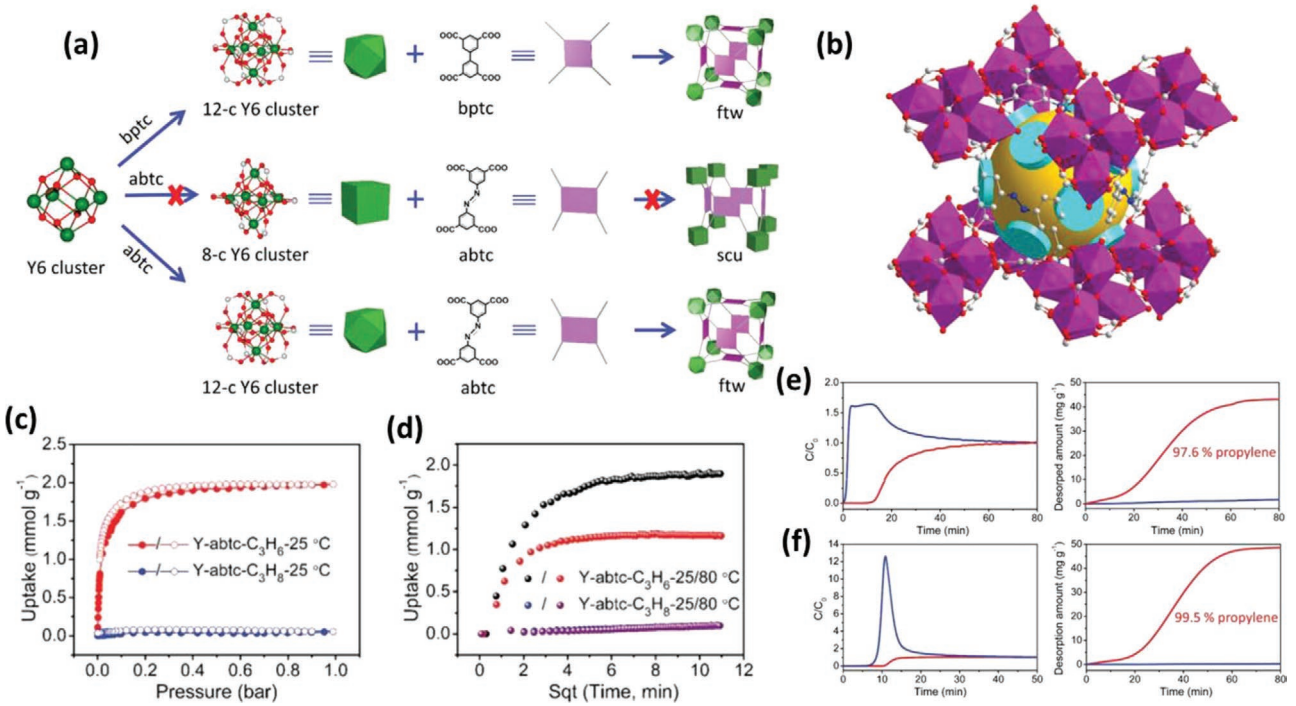

Figure 11. a) Topology-directed design strategy for the tuning of pore aperture of Y-ftw-MOFs. b) Crystal structure of Y-abtc showing its cate-like pores. c) Single-component adsorption isotherms for propane and propylene by Y-abtc at 298 K up to 1 bar. d) Time-dependent adsorption of propane and propylene by Y-abtc at 298 and 353 K and 0.8 bar. e,f) Column breakthrough curves showing that propylene purities of 97.6% and 99.5% were obtained for 50:50 (e) and 10:90 (f) propylene/propane mixtures. Reproduced with permission.[37] Copyright 2018, Wiley-VCH.

to the existence of charge-balancing cations inside the pores of the latter. Y-abtc has the optimum pore aperture to adsorb propylene only while fully excluding propane. Adsorption isotherms and kinetic measurements confirmed that the separation was based on selective size-exclusion rather than kinetic separation as there was no indication of propane uptake at an elevated temperature (from 298 to 353 K). Importantly, multicomponent column breakthrough measurements revealed that the material was capable of producing propylene with 99.5% purity starting from propane/propylene mixtures, well meeting the requirement for the production of polypropylene. Further analysis confirmed that the pore aperture of Y-abtc was regulated by charge balancing cations, which served as an additional regulator supplementary to the choice of ligand. In an independent study, Eddaoudi et al. reported the separation of propane and propylene by ftw-MOF-abtc (Tb-abtc), which features the same connectivity as that of the Y-abtc.[83] It exhibits highly efficient kinetic separation of propane and propylene at room temperature. It is worth to note that the material adsorbs similar amounts of propane and propylene under equilibrium conditions. The difference in adsorption behavior for Tb-abtc and Y-abtc is likely due to the use of different metal ions.

Tailored MOF pore environment, either achieved by rational design of SBUs and ligands or through post-synthetic modifications, can lead to separation with high efficiency. Recently, Zhang et al. demonstrated the boost of propylene/propane selectivity by selective aerobic oxidation of an existing MOF.[84] The authors started from MAF-23 ($Zn_2(btm)_2$, H_2btm = bis(5-methyl-1H-1,2,4-triazol-3-yl)methane), which showed similar adsorption behavior (adsorption capacity and kinetics) toward propane and propylene, and no noticeable separation was observed from multicomponent breakthrough measurements. Interestingly, the btm^{2-} ligands in MAF-23 can be selectively oxidized by oxygen to form btk^{2-} (H_2btk = bis(5-methyl-1,2,4-triazol-3-yl)methanone), resulting in a new MOF, MAF-23-O. The pristine crystal structure of MAF-23 was retained in MAF-23-O with half amount of btm^{2-} oxidized to btm^{2-}. Single component adsorption isotherms, adsorption kinetics, and multicomponent column breakthrough measurements revealed that MAF-23-O was capable of effectively separating propane and propylene, in contrast to its parent structure MAF-23. The propylene/propane kinetic selectivity was 112.3 for MAF-23-O, which is two orders of magnitude higher than that of the pristine compound. In addition, the thermodynamic selectivity was also largely enhanced due to the formation of the carbonyl bridges. The authors reported a propylene/propane selectivity of 15 for MAF-23-O from breakthrough experiments, which is higher than that of MOF-74-Co and KAUST-7 under identical conditions. This study demonstrated that the kinetic and thermodynamic selectivity for the separation of propane and propylene can be improved substantially through post-synthetic modification which led to the subtle changes in pore size and pore environment.

3.4. C_4 Olefins

C_4 olefins, including 1,3-butadiene (C_4H_6), 1-butene (n-C_4H_8), and isobutene (i-C_4H_8), are all important raw materials in chemical industry. Among them, C_4H_6 is of particular value

because of its wide use for the production of synthetic rubber. The stream of C_4 olefins, including 30–60% C_4H_6, 10–20% n-C_4H_8, 10–30% i-C_4H_8, as well as a small amount of butane, is formed during oil refinement.[85] To obtain polymer-grade C_4H_6 (purity >99.5%), it needs to be separated and purified from the C_4 mixtures. Current separation technology relies on distillation at relatively high pressure and elevated temperature, and suffers from intensive energy consumption as well as the risk of polymerization of C_4H_6 at high temperature. Adsorptive separation of C_4 olefins represents a challenging task because of the very similar size, shape, and physical properties of the adsorbates. MOFs have shown superior performance for this separation process thanks to their exceptional tunability in their pore structure and surface functionality that allow the accommodation of different separation mechanisms, including thermodynamic separation, kinetic separation, controlling gas conformation, and guest-responsive mechanism.[86–88] In general, MOFs with OMSs show preferential adsorption toward C_4 olefins due to the π-complexation interactions, which help discriminating them from butane. However, these MOFs do not exhibit separation capability between C_4 olefins. Kitagawa et al. reported a flexible MOF, Zn(NO_2ip)(dpe) (also termed as SD-65, NO_2ip = 5-nitroisophthalate, dpe = 1,2-di(4-pyridyl) ethylene), which showed specific recognition toward 1,3-butadiene (C_4H_6) over other accompanied impurities.[89] Single-component adsorption revealed a stepwise adsorption of SD-65 toward C_4H_6 at 298 K, with no adsorption before 50 kPa and a steep increase between 50–70 kPa reaching a saturated uptake of ≈1.79 mmol g^{-1} up to 100 kPa. In contrast, SD-65 exhibited essentially no uptake for any other C_4 olefins or paraffins at 298 K up to 100 kPa. This result may be attributed to the suitable pore size and specific adsorbate–MOF interaction that induced the structural change and the subsequent guest accommodation, which is not uncommon for flexible MOFs. Although excellent adsorption selectivity was observed for SD-65 from single-component adsorption isotherms, its efficient separation of 1,3-butadiene (C_4H_6) from mixed gases would not be expected. This is due to the fact that the experimental conditions for a single gas and gas mixture are very different. As a result, the adsorption selectivity calculated from single-component adsorption results would partially sacrifice under mixed gas conditions. This was confirmed by the multicomponent breakthrough measurements where a clean separation of C_4H_6 from other C_4 olefins/paraffins was not observed.

To develop suitable MOFs with optimal pore structure and functionality for efficient separation of C_4 olefins, Xing et al. applied reticular chemistry to the anion-pillared ultramicroporous MOFs derived from the SIFSIX series to fine tune their pore aperture.[90] The pore size of these MOFs could be adjusted by judicious design/selection of organic ligands (dipyridyl derivatives), and can be further fine-tuned by the increment of 0.2 Å by altering the anion pillars. Adsorption and separation performance of C_4 olefins were evaluated on a series of anion-pillared MOFs, including TIFSIX-2-Cu-i, SIFSIX-2-Cu-i, GeFSIX-2-Cu-i, NbFSIX-2-Cu-i, and GeFSIX-14-Cu-i. These structures have the same connectivity as that of the SIFSIX series and contain fluorine arrays along the 1D channels, but their pore sizes are different. They all exhibit certain separation capabilities for C_4 olefins. Specifically, it is worth mentioning that one of the structures, GeFSIX-14-Cu-i, showed selective adsorption of C_4H_6 over both i-C_4H_8 and n-C_4H_8. It adsorbed 2.67 mmol g^{-1} of C_4H_6 at 298 K and 1 bar, but its adsorption capacity for the other two gases was negligible, especially at relatively low pressure. This was a result of the contracted pore size and the synergetic effect of C_4H_6 loading and the rotation of the organic ligands, which allowed the accommodation of C_4H_6 but excluded the other two gases. Multicomponent column breakthrough measurements confirmed the capability of GeFSIX-14-Cu-i for the purification of C_4H_6.

In general, the above-mentioned materials show capability of selectively adsorbing C_4H_6 from the C_4 olefin mixtures. However, such an adsorptive separation pathway is not optimum as the subsequent desorption process by heating, to produce pure C_4H_6, may induce polymerization. In addition, multiple adsorption–desorption cycles are needed to achieve the required C_4H_6 purity. Thus, an ideal adsorbent would preferentially adsorb C_4 olefins other than C_4H_6 so that it would elute out from the adsorption bed as a pure product. To this end, Zhang et al. reported a state-of-the-art work for the separation of C_4 olefins by $Zn_2(btm)_2$ (H_2btm = bis(5-methyl-1H-1,2,4-triazol-3-yl)methane) (**Figure 12**).[85] The authors studied the adsorption and separation properties for C_4 olefins on ten selected MOF materials

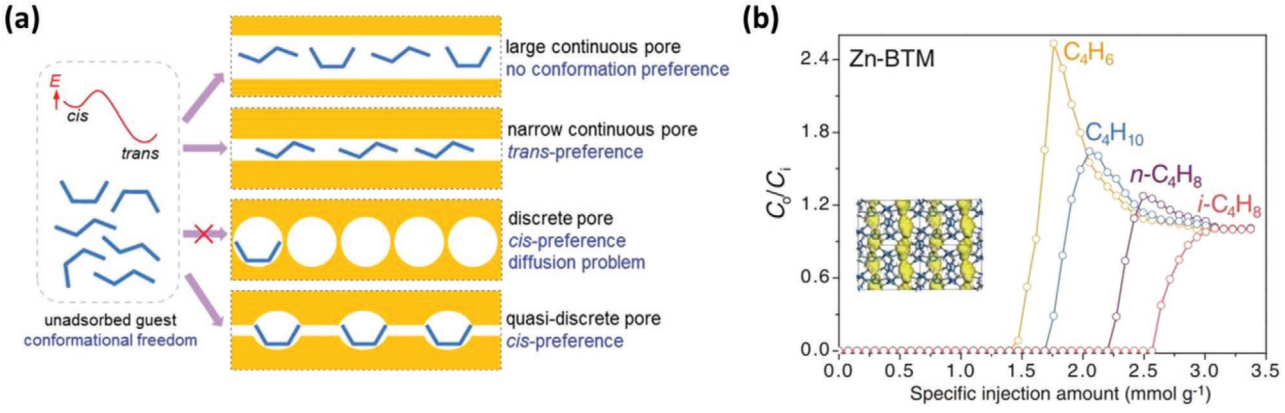

Figure 12. a) Controlling the guest conformations by variation of the pore size, shape, and dimensionality. b) Mixture breakthrough curves for C_4 hydrocarbons on Zn-BTM for a 1:1:1:1 C_4H_6/n-C_4H_8/i-C_4H_8/C_4H_{10} mixture. Reproduced with permission.[85] Copyright 2017, AAAS.

with various pore sizes, pore shapes, and surface functionalities, by multicomponent column breakthrough experiments of an equimolar mixture of C_4H_{10}, n-C_4H_8, i-C_4H_8, and C_4H_6. Typically, for MOFs with OMSs, the breakthrough time follows the sequence of C_4H_{10} << n-C_4H_8 < i-C_4H_8 < C_4H_6, which is reasonable considering the relative coordination strength between these molecules and the OMSs. Separation performances of selected hydrophobic MOFs were relatively poor as the adsorbates have very similar polarity and polarizability. In contrast, for MOFs with hydrophilic pores, their separation behavior relates closely to the pore structure. It is noteworthy that Zn-BTM possessing quasi-discrete cavities and suitable pore size exhibited preferential adsorption of C_4 olefins other than C_4H_6, with breakthrough times in the sequence of C_4H_6 < C_4H_{10} < n-C_4H_8 < i-C_4H_8, which were very different from the behavior of other adsorbents. Further analysis revealed that Zn-BTM could directly produce C_4H_6 with a purity of 99.9%, well meeting the required purity for polymer production, without the need of additional desorption processes. Guest-loaded crystal structure analysis and DFT computational calculations and modeling uncovered that the selective adsorption behavior is a result of the conformation control of the guest molecules and the matching between the guest and the pore structure.

4. Separation of Alkane Isomers

4.1. Background and Representative Examples of Thermodynamic Separation

The separation of alkane isomers, particularly C_5-C_7, represents an important yet challenging process in petrochemical industry during oil refinement, in order to produce premium gasoline components with high octane rating.[1] A stream of alkanes with different degree of branching are produced upon catalytic isomerization reactions. Dibranched alkanes are superior blending components for premium gasoline, followed by monobranched isomers, and the linear counterparts are of the lowest value due to their relatively low research octane number (RON). Thus, in the subsequent step, linear alkanes or ideally both linear and monobranched alkanes should be removed from the mixture, producing branched or ideally dibranched isomers as highly valuable gasoline components. The adsorptive separation of these nonpolar alkanes are challenging as they are similar in chemical functionality and molecular dimensions. In light of the fact that the molecules to be separated have different shapes, a possible solution would be to develop shape-selective adsorbent materials so as to achieve efficient separation.[91] The benchmark adsorbent material for the separation of alkane isomers is zeolite 5A (LTA), which is capable of splitting branched alkanes from their linear isomers through selective size exclusion.[3] Zeolite 5A has a BET surface area of ≈500 m^2 g^{-1}, and a pore aperture of ≈5 Å, with adsorption capacities of 17 and 8 wt% for nHEX at 30 and 150 °C. Attributed to its suitable pore size, Zeolite 5A adsorbs linear alkanes only but fully excludes any branched isomers. This makes zeolite 5A the only adsorbent so far that has been industrially implemented for the separation of alkane isomers. However, it is noteworthy that adsorptive separation by zeolite 5A has not been widely applied as a replacement for distillations, but only used sporadically in some refinery as a supplement. This is due to the fact that the separation performance of zeolite 5A is not fully meeting the requirement by industrial process. The relatively low adsorption capacity of zeolite 5A limits its separation efficiency. More importantly, the incapability of adsorbing any branched alkanes prevents its use for achieving further improved RON by differentiating mono- and di-branched isomers.

The exploration of MOFs for separation of alkane isomers started early in 2006, where Chen and co-workers reported the separation of C_5 and C_6 alkane isomers using MOF-508 as the stationary phase of gas chromatography.[92] Different retention times were observed for each alkane isomers, which was attributed to the different van der Waals interactions arising from subtle size- and shape-selective matching. In another pioneering work, Long et al. performed a comprehensive study of hexane isomers separation on $Fe_2(BDP)_3$,[93] and made a comparison with many other reported adsorbent materials, including both zeolites and MOFs, with respect to their separation capability for hexane isomers. Experimental and simulation results indicate that $Fe_2(BDP)_3$ can finely separate hexane isomers of different degree of branching, outperforming traditional adsorbents and previous reported MOFs. $Fe_3(BDP)_3$ features 1D triangular channels with aperture size that is large enough to accommodate all hexane isomers without notable diffusion restrictions. The separation of hexane isomers on $Fe_3(BDP)_3$ is essentially thermodynamically controlled, supported by adsorption enthalpy of each isomer and the profiles of their breakthrough curve. The authors concluded that the 1D channels provide stronger van der Waals contacts for linear alkanes, while for dibranched isomers, the contacts are not maximized.

4.2. Kinetic Separation

Tremendous progress has been made in efficient separation of alkane isomers by MOFs through size/shape discrimination. One early and prototype example is ZIF-8, which has been extensively studied for this separation process.[3,94–97] ZIF-8 is a representative member of the zeolitic imidazolate framework (ZIF) family with remarkable thermal and chemical stability. It features a sodalite (SOD)-type framework with cage-like pores including large cavities (≈11.4 Å) connected through narrow six-membered-ring windows (≈3.4 Å). The small cage window in ZIF-8 does not show a sharp cutoff at ≈3.4 Å with respect to guest inclusion due to its structural flexibility. It has been experimentally demonstrated that ZIF-8 can accommodate not only linear alkanes, but also their branched isomers, and even molecules as large as 1,2,4-trimethylbenzene (124TMB).[98] However, notable differences have been observed for the adsorption behaviors of alkane isomers on ZIF-8 under various conditions, indicating that its adsorption is highly dependent on the pressure, temperature, and other experimental parameters. Yan et al. applied a ZIF-8-coated capillary for the separation of linear alkanes from their branched isomers using gas chromatography, which showed clear separation between nHEX (n-hexane) and other branched isomers.[97] The authors concluded that the separation is based on selective size-exclusion and the negligible retention of monobranched isomer is due

to the adsorption of the linear part of the hydrocarbon chain in the pore mouth. Zhang et al. investigated the adsorption and separation of nHEX and 2MP (2-methylpentane) by ZIF-8 with liquid adsorption systems, and compared it with zeolite 5A.[95] In an isooctane solution with 15% nHEX, ZIF-8 showed an adsorption capacity of 51 wt% at 25 °C, substantially higher than that of zeolite 5A (15 wt%). This could be attributed to its larger BET surface area (1285 m^2 g^{-1}) than that of the latter (515 m^2 g^{-1}). In contrast, ZIF-8 adsorbs 9 wt% of 2MP under identical conditions, notably lower than its uptake toward nHEX. For both isomers, adsorption reaches equilibrium within 10–15 min, without significant diffusion restrictions. Breakthrough experiments for binary mixtures suggest that ZIF-8 can effectively separate nHEX and 2MP, with substantially longer retention time for nHEX than that of 2MP. Pirngruber et al. carried out another comparative study of hexane isomer adsorption on ZIF-8 and zeolite 5A, with expanded adsorbate systems, including nHEX, 3MP (3-methylpentane), and 22DMB (2,2-dimethylbutane).[3] Breakthrough measurements of binary mixtures (nHEX/3MP, nHEX/22DMB, or 3MP/22DMB) demonstrated that ZIF-8 was capable of effectively separating nHEX/3MP and nHEX/22DMB, with slight discrimination for 3MP/22DMB. In contrast, zeolite 5A showed essentially no separation for 3MP/22DMB as neither of them was allowed to diffuse into its pores. The authors concluded that the monobranched isomer (3MP) is at the edge of the cutoff, meaning that its adsorption is possible but subject to severe diffusional restrictions. With experimental proofs, they believed that 3MP was not only adsorbed at the pore mouth, but instead, it genuinely entered into the sodalite cages of ZIF-8, although with slow kinetics. In addition to diffusion limitations, 3MP was also thermodynamically less-favored compared to nHEX. Thus, the separation of nHEX and 3MP by ZIF-8 is both thermodynamically and kinetically controlled. With combined experimental proof and theoretical explanation, Rothenberg et al. confirmed the conclusion by Pirngruber et al. that monobranched hexanes could be adsorbed by ZIF-8, but was thermodynamically and kinetically less favored compared to nHEX.[94] Single-component vapor adsorption isotherms at 373 K displayed substantial uptake of nHEX, 3MP, and 23DMB by ZIF-8, but 22DMB was almost excluded. The measured differential heats of adsorption followed the sequence of nHEX > 3MP > 23DMB > 22DMB. The results indicated the potential capability of ZIF-8 for the full separation of 22DMB from the hexane mixtures. From these studies, it is clear that monobranched alkanes are at the edge of the cutoff for ZIF-8 with respect to the inclusion of alkane isomers. By optimizing the experimental conditions (temperature/pressure), ZIF-8 can be used as an adsorbent either for the full separation between linear alkanes and branched isomers, or for splitting dibranched alkanes from the mixture.

In another early study reported by Chen et al., Zn(BDC)$(Dabco)_{0.5}$ was used for the separation of nHEX from its branched isomers.[99] This MOF has two types of intersecting channels with cross sections of ≈7.5 Å × 7.5 Å and 3.8 Å × 4.7 Å, respectively. The authors speculated that the larger channels are accessible to all hexane isomers, but the smaller ones are accessible to nHEX only and will exclude the other two isomers. This was supported by experimental adsorption results, and the adsorption capacity for nHEX was substantially higher than that of 3MP and 22DMB. Multicomponent column breakthrough measurements confirmed that the MOF was capable of well separating nHEX from its branched isomers. Zhao et al. evaluated the adsorption of nHEX, 3MP, and 22DMB on $Zn_2(Hbdc)_2(dmtrz)_2$ (H_2bdc = 1,4-benzenedicarboxylic acid, Hdmtrz = 3,5-dimethyl-1H,1,2,4-triazole).[100] The MOF possesses 1D channels with diameter of 6.7 Å. Single-component vapor adsorption isotherms revealed that it adsorbs similar amounts of nHEX (13.3 wt%) and 3MP (12.1 wt%), but substantially less 22DMB (3.5 wt%). Gas chromatography measurements using a $Zn_2(Hbdc)_2(dmtrz)_2$-filled column indicated that 22DMB was nicely separated from the other two isomers. Though adsorption kinetics data were not reported, it is reasonable to speculate that the separation is kinetically controlled, or a result of both thermodynamic and kinetic effect. Silva et al. carried out an experimental screening on a series of rigid MOFs, including MIL-100(Cr), MIL-125(Ti)-NH_2, and MIL-127(Fe), and found that MIL-127(Fe) exhibits a size-exclusion-based separation for linear and branched hexanes due to its suitable pore size.[101] In the multicomponent column breakthrough experiments, only nHEX showed noticeable retention while other branched isomers eluted immediately out from the column. More recently, Lv et al. reported the adsorption and separation of hexane isomers on a hydrophobic MOF, $Fe_3(\mu_3\text{-O})](6fdca)_3$, built on a fluorinated linker.[102] While equilibrium adsorption isotherms indicated the compound could accommodate all three hexane isomers (nHEX, 3MP, 22DMB), they displayed distinctly different adsorption kinetics. The adsorption of 22DMB was much slower than its other two isomers. Multicomponent breakthrough experiments also suggested that it was capable of separating hexane isomers as a function of degree of branching.

4.3. Size-Exclusion-Based Separation

In the above-mentioned examples, while some MOFs have demonstrated potential for the separation of alkane isomers, they usually suffer from relatively low adsorption capacity or selectivity. This could be partly because such studies have focused more on general, rather than targeted, properties of the MOF compounds, such as their performance for a specific separation process. Over the past few years, significant progresses have been made in designing task-specific MOFs by fine-tuning their pore structure (pore size and pore shape) through topology-directed approach. Eddaoudi et al. reported the ultra-tuning of rare-earth metal based MOFs with fcu topology (RE-fcu-MOFs) for the separation of alkane isomers (**Figure 13**).[103] RE-fcu-MOFs are very similar to the Zr-based MOFs with fcu topology, that is, the UiO series. They feature similar SBUs and connectivity, but RE-fcu-MOFs have anionic backbone with balancing cations inside the pores, while the Zr-based MOFs are neutral frameworks. The authors synthesized a series of isoreticular compounds by combining different RE metals (i.e., Y, Tb, Yb, Sm, Er, Ho, Dy, Gd) and linear bifunctional linkers. Through a careful screening process, they found Y-fum (fum = fumarate) has the optimal pore dimensions for the separation of alkane isomers. Y-fum possesses two types of cages with tetrahedral and octahedral geometry, respectively. Both cages are accessible through triangular windows with a diameter of 4.7 Å, which

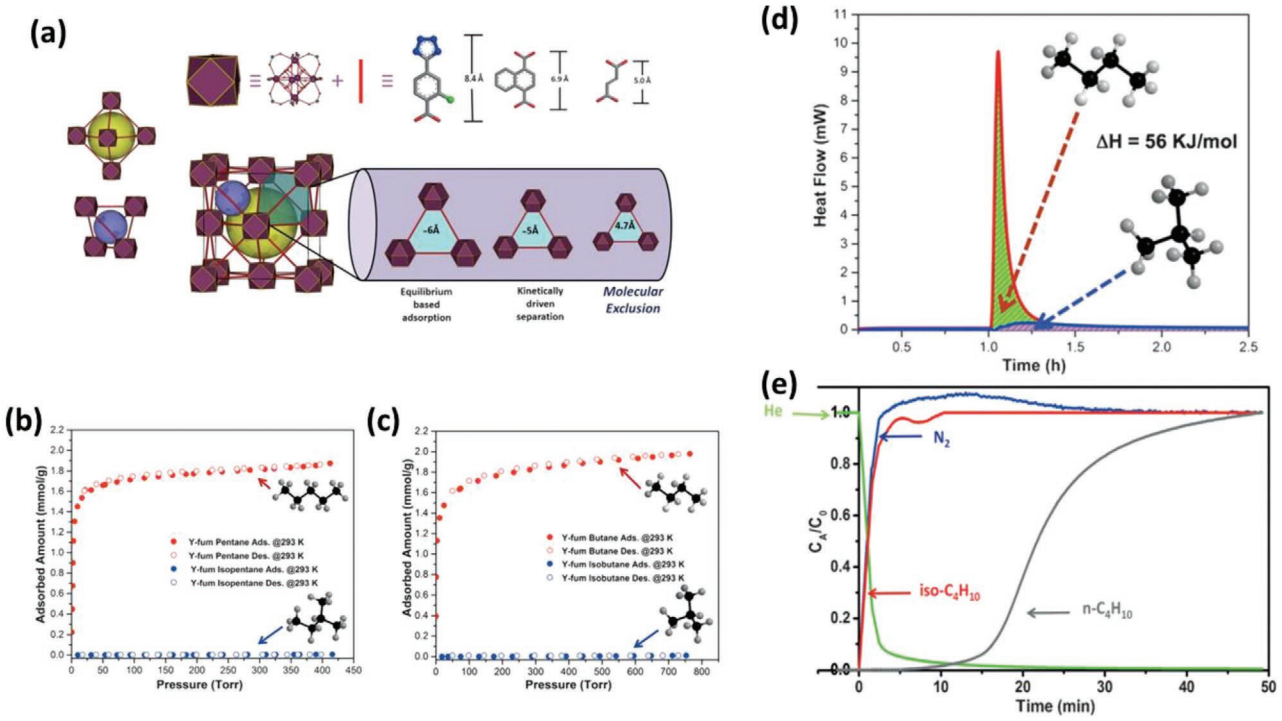

Figure 13. a) Schematic representation of the components of the RE-fcu-MOFs platform including three possible organic linkers of different length for tuning the pore aperture of the MOFs. b,c) Sorption isotherms for pentane/isopentane (b) and butane/isobutane (c) at 293 K by Y-fum. d) Heat flow for the adsorption of n-butane and isobutene on Y-fum obtained by TG-DSC analysis. e) Column breakthrough test for the adsorption of mixed n-butane (5%) and isobutene (5%) in balance with nitrogen. Reproduced with permission.[103] Copyright 2015, Wiley-VCH.

falls right between the kinetic diameters of linear and monobranched alkanes. Y-fum has a BET surface area of 691 m^2 g^{-1} and adsorbs 1.8 and 2.0 mmol g^{-1} of n-pentane and n-butane at 293 K, respectively, with fast adsorption kinetics. In contrast, it adsorbs essentially no isopentane or isobutane under identical conditions, indicating its aperture size serves as a perfect cutoff for the full separation of linear and branched isomers. The adsorption enthalpy of n-butane was found to be 56 kJ mol^{-1} from simultaneous thermal gravimetric and calorimetric measurements (TG-DSC), while no noticeable exothermic effect was observed for isobutane, confirming its molecular sieving behavior. This was further evidenced by column breakthrough experiments for binary mixtures, where isobutane showed no retention while *n*-butane was retained in the column for a markedly longer time. It is noteworthy that the authors reasoned Y-fum outperformed zeolite 5A because appreciable amounts of monobranched alkanes (i.e., isopentane and isobutane) were found to be adsorbed in the α cage of the latter, thus, lessening its separation efficiency. In contrast, Y-fum showed absolutely no adsorption of monobranched alkanes. In another study, using a slightly longer linker 1,4-NDC (1,4-naphthalenedicarboxylate), the authors obtained Y-1,4-NDC with similar structure but slightly larger pore aperture (≈5 Å).[104] Experimental results showed that Y-1,4-NDC adsorbed almost identical amounts of n-pentane and isopentane under equilibrium conditions, but faster adsorption kinetics for the former than its monobranched isomer, indicating its kinetically controlled separation capability.

Other than the above-mentioned fcu-type structures, MOFs with ftw topology represent another group of MOFs that are extensively investigated and are promising for molecular separation.[105] MOFs with ftw-type structure are normally built on 12-connected hexanuclear M_6 (M = Zr, Y, Tb, etc.) SBUs and 4-connected square-shaped (or rectangular) tetra-functional (usually tetracarboxylates) linkers. Similar structures with less connected M_6 SBUs (i.e., 8, 6, 4-connected) adopt ftw-derivative topology such as scu and lvt.[106] ftw-type MOFs are generally thermally robust and resistant to water or moisture, due to the strong M-O bonds and robust 12-connected SBUs. The ftw-type MOF structures have cubic cage-like pores connected through small windows which are ideal pore system for hydrocarbon separation: The large chambers guarantee high adsorption capacity, while small windows may function as "gates" that can discriminate adsorbates with different size, shape, or functionality. In addition, pore aperture of an ftw-type MOF is essentially determined by the dimension of the linker, or more precisely, the distance between adjacent carboxylates. Thus, through judicious ligand design based on reticular chemistry, one can fine tune the pore aperture of ftw-MOFs without altering their connectivity or pore shape. Zhou et al. and many other research groups have made enormous progresses in the preparation, structure, and potential applications of zirconium-based ftw-type MOFs (Zr-ftw-MOFs). However, most of these structures are constructed from large square-shaped linkers such as porphyrin- or pyrene-based molecules. With very large pores, they are not optimal for the separation of light hydrocarbons. In order to reduce the pore aperture of Zr-ftw-MOFs and explore their potential for the separation of alkane isomers, Li et al. attempted to develop MOFs with deliberately selected isophthalate-based tetratopic linkers with appropriate dimensions for the purpose of reducing the distance between adjacent

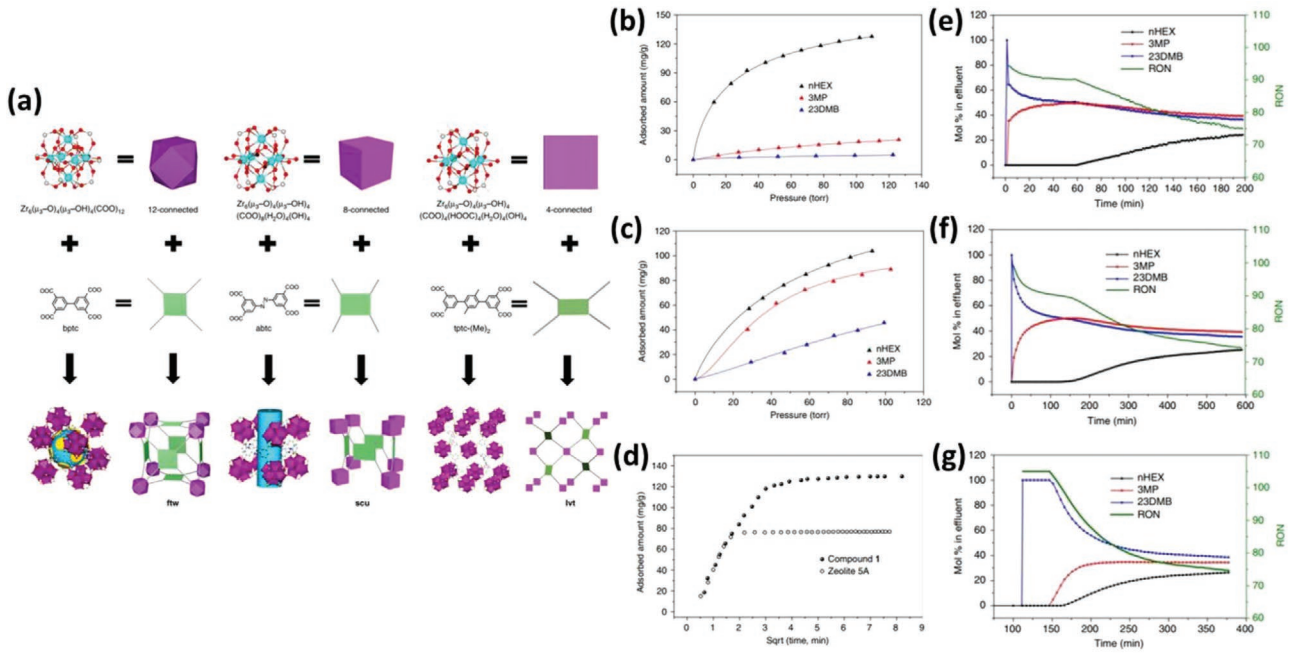

Figure 14. a) Topology-directed design of Zr-MOFs built on planar tetracarboxylate ligands. b,c) Adsorption isotherms of nHEX, 3MP, and 23DMB by Zr-bptc (b) and Zr-abtc (c) at 413 K. d) Comparison of time-dependent adsorption of nHEX on zeolite 5A and Zr-bptc at 413 K and 100 torr. e–g) Column breakthrough curves for a ternary mixture of nHEX, 3MP, and 22DMB for zeolite 5A (e), Zr-bptc (f), and Zr-abtc (g) at 413 K under identical conditions. Reproduced with permission.[106] Copyright 2018, Springer Nature.

SBUs and consequently the pore aperture.[106] A series of three Zr-MOFs built on three linkers with similar functionality and geometry but different aspect ratios (i.e., bptc, abtc, tptc) were synthesized and characterized (**Figure 14**). The three MOFs adopt ftw-, scu-, and lvt-type framework, respectively, with the three ligands bptc, abtc, and tptc in ascending aspect ratios. Both Zr-bptc and Zr-abtc structures are highly robust with BET surface areas of 1030 and 1318 $m^2\ g^{-1}$, respectively, while the lvt-type Zr-tptc is structurally fragile, likely due to the low connectivity of SBUs (4-connected). Zr-bptc features the cage-like pores for ftw-type MOFs with pore aperture of ≈4.5 Å. Behaving similarly to zeolite 5A, it adsorbs linear alkanes but excluded branched isomers. Notably, it has an adsorption capacity of 13 wt% of nHEX at 150 °C, significantly higher than that of zeolite 5A under identical conditions (≈8 wt%). This could be attributed to its noticeably higher surface area compared to that of zeolite 5A. The separation capability of Zr-bptc was confirmed by multicomponent column breakthrough measurements which demonstrated substantial retention for nHEX while its branched isomers eluted immediately out of the column. The experimental results also suggest that Zr-bptc has a significantly higher dynamic adsorption capacity than that of zeolite 5A under identical conditions of the gas mixture. The separation mechanism of selective size exclusion was supported by additional computational calculation and simulations. Derived from ftw-type Zr-bptc, Zr-abtc features 8-connected SBUs and scu-type structure, where the cage-like pores transform to 1D channels of ≈7 Å diameter. As expected, it accommodates all C_6 alkane isomers but thermodynamically favors nHEX because of its more sufficient contacts with the 1D channels, acting similarly to $Fe_2(BDP)_3$.[93] However, noticeable diffusional limitations were observed for dibranched alkane isomers during their adsorption in Zr-abtc, indicating the separation was partly kinetically controlled. This also explains why the separation selectivity of Zr-abtc is higher than that of $Fe_2(BDP)_3$ which shows free diffusion for all isomers with different degrees of branching.

In addition to topology-directed tuning of MOF pore aperture, another important approach to achieve highly efficient separation of alkane isomers is to design flexible MOFs with unique separation selectivity. Adsorption by MOFs with structural flexibility is generally dependent on pressure, temperature, and adsorbates, which would sometimes lead to unexpected adsorption and separation properties. Mendes et al. reported the adsorption and separation of hexane isomers on a functionalized flexible MOF, MIL-53(Fe)-$(CF3)_2$.[107] While it adsorbed similar amounts of nHEX, 3MP, and 22DMB under equilibrium conditions, clear separation under multicomponent conditions was observed. For a ternary mixture of nHEX, 3MP, and 22DMB with a total pressure of 1 kPa at 313 K, MIL-53(Fe)-$(CF3)_2$ demonstrated a complete sieving of 22DMB from the other two isomers. With additional adsorption and computational evidences, the authors concluded that it was a kinetically controlled separation, as 22DMB showed slow adsorption kinetics under such conditions. However, it should be noted that the separation performance was highly temperature and pressure dependent, which may vary significantly at different temperatures or pressures. This study provides some clue on making use of flexible MOFs for this challenging separation.

Another important work of using flexible MOFs was reported by Li and co-workers focusing on the temperature-programmed separation of alkane isomers by Ca(H_2tcpb).[108] Ca(H_2tcpb) is a 3D structure built on CaO_6 octahedra connected through H_2tcpb^{2-} linkers, possessing 1D open channels with a diameter

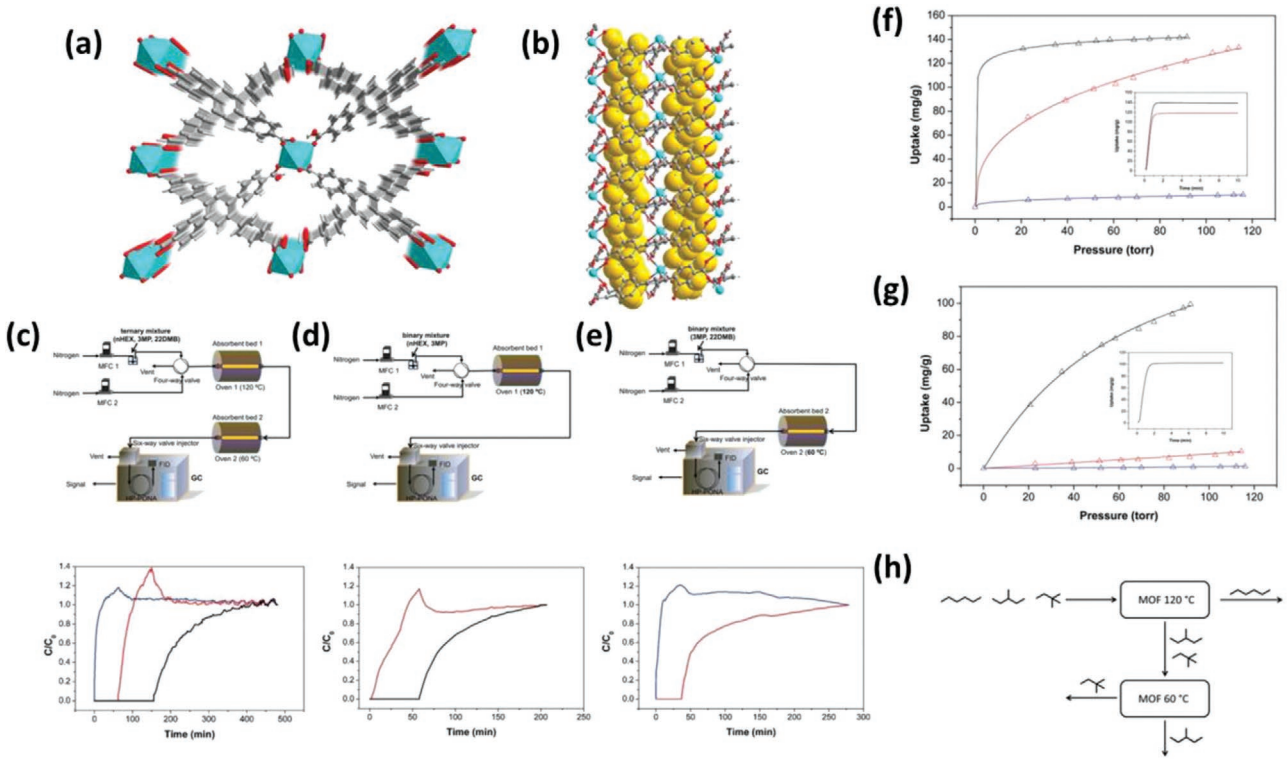

Figure 15. a) Crystal structure of Ca(H_2tcpb). b) 1D channels of Ca(H_2tcpb) depicted by adsorption simulations. c–e) Multicomponent column breakthrough results for a ternary mixture of nHEX, 3MP, and 22DMB at 60 and 120 °C by two-column system (c), a binary mixture of nHEX and 3MP at 120 °C (d), and a binary mixture of 3MP and 22DMB at 60 °C (e). f,g) Adsorption isotherms of nHEX, 3MP, and 22DMB at 60 °C (f) and 120 °C (g). h) Schematic representation of the temperature-programmed separation of C6 alkane isomers by a two-column system. Reproduced with permission.[108] Copyright 2018, Royal Society of Chemistry.

of ≈5.5 Å (**Figure 15**). The pore aperture falls close to the molecular size of monobranched alkanes. Interestingly, under ambient vapor pressure, the adsorption of hexane isomers on Ca(H_2tcpb) is highly dependent on temperature. It adsorbs nHEX only at 120 °C, and can accommodate both nHEX and 3MP at 60 °C but fully excludes 22DMB. However, at 30 °C, it is capable of adsorbing all three isomers. Thus, Ca(H_2tcpb) acts as a molecular sieve for linear and branched alkanes at 120 °C, while at 60 °C it is capable of sieving dibranched isomer from linear and monobranched alkanes. Multicomponent column breakthrough measurements confirmed its separation capability, showing clear separation of nHEX/3MP and 3MP/22DMB at 120 and 60 °C, respectively. More importantly, the authors developed a temperature-programmed two-column system, with one column at 120 °C and the other at 60 °C, which showed a total separation of a ternary mixture into three individual components. Further X-ray diffraction analysis revealed that the temperature- and adsorbate-dependent adsorption behavior of Ca(H_2tcpb) was a result of its structural flexibility which led to change of pore aperture at different temperatures and upon adsorption of different guests. It is noteworthy that, similar to that of MIL-53(Fe)-$(CF3)_2$, the separation property of Ca(H_2tcpb) is retained at a specific range of temperature and pressure.

More recently, Yu et al. reported the total separation of dibranched alkanes from their linear and monobranched isomers at ambient temperature and pressure by a rigid MOF, Al(bttotb) (H_3bttotb = 4,4′,4″-(benzene-1,3,5-triyltris(oxy))tribenzoicacid).[109] It has 1D channels with a diameter of ≈5.6 Å, comparable to the kinetic diameter of monobranched alkanes. The MOF adsorbs linear and monobranched hexanes with relatively fast kinetics at room temperature, but fully excludes dibranched 22DMB. Multicomponent column breakthrough experiments confirm its capability of sieving dibranched alkanes from the alkane mixture of isomers of different degrees of branching. This represents the first adsorbent with rigid structure that is capable of separating dibranched alkanes from their linear and monobranched isomers through selective size exclusion. Single crystal X-ray diffraction analysis and computational simulations on guest-included crystals provided explanations on the alkane adsorption–separation at the molecular level.

5. Separation of C_8 Alkylaromatic Hydrocarbons

C_8 alkylaromatic hydrocarbons, including *p*-xylene (*p*X), *o*-xylene (*o*X), *m*-xylene (*m*X), ethylbenzene (EB), and styrene (ST), are all important chemical raw materials wisely used in various aspects.[110] Particularly, *p*X is the starting material for terephthalic acid, which is further used as feedstock for the production of polyesters and polyamides, such as polyethylene terephthalate (PET). *p*X is mainly generated from catalytic reforming during oil refinement, coexisting with its other isomers. Current technologies of separating C_8 alkylaromatics include

distillation, crystallization, and adsorptive separation. In comparison, separation by selective adsorption is potentially more energy efficient. However, adsorptive separation of C_8 alkylaromatics with high efficiency represents a great challenge due to their similar physical properties, including molecular shape, size, and functionality. FAU-type zeolite X and Y are the main adsorbents currently employed for the separation of C_8 aromatics in industry, but with relatively low selectivity and limited adsorption kinetics.[6] A number of MOFs have been tested for possible separation of C_8 aromatics and promising results have been obtained for some of them. Long and co-workers reported the utilization of MOFs with OMS for the separation of xylene isomers and EB.[111] They found MOF-74-Co with a high density of coordinatively unsaturated Co(II) centers along its 1D channels was capable of distinguishing among the four isomers. Single component adsorption and multicomponent column breakthrough measurements revealed the separation was driven thermodynamically as a result of different strength of adsorption affinity between the framework and each adsorbate. The binding affinities for MOF-74-Co followed the sequence of *o*X > EB > *m*X > *p*X. The selective adsorption among these molecules was a result of the framework–guest interactions, the corresponding framework distortion, as well as adsorbate–adsorbate interactions, as evidenced by single-crystal X-ray diffraction analysis. It was observed that upon the adsorption of the two strongest binding isomers *o*X and EB, distortion of the channels occurred to accommodate additional guest molecules, which was attributed to the interplay between the energetic penalty incurred upon framework deformation and the thermodynamic stability gained through enhanced framework–guest interactions and the adsorption of additional molecules upon distortion. This indicates that framework flexibility could have played an important role for the observed selective adsorption.

Several flexible MOFs were also found to show discrimination among C_8 aromatic hydrocarbons. Guo et al. investigated the adsorption of xylene isomers on MIL-53(Cr) and noted that the material was highly OX selective.[112] Its separation capability was experimentally confirmed by multicomponent breakthrough measurements as well as mixed liquid phase adsorption. In addition, the material exhibited exceptional adsorption capacity for *o*X (>80 wt%). Its preferred adsorption toward *o*X was a result of both entropy and enthalpy effects. These findings were supported by another independent study carried out by Nair and co-workers,[113] where the authors studied the quaternary liquid-phase breakthrough measurements in MIL-53 materials under industrially relevant xylene feeds and operating conditions. It was demonstrated that the material was capable of separating *o*X from other three isomers (*p*X, *m*X, EB). The selective adsorption of *o*X was attributed to its high packing efficiency as well as its preferential interaction with the organic linker. More recently, Zhang et al. reported the utilization of a flexible MOF $Cu_2(pypz)_2$ (MAF-36, Hpypz = 4-(1H-pyrazol-4-yl)pyridine) for highly efficient separation of xylenes.[114] The material was synthesized using *p*X as a cosolvent and the as-synthesized compound had *p*X inside its 1D channels as guest molecules. The framework underwent structure transformation upon removal of *p*X from the chwannels. However, because of its structural flexibility and the so-called shape-memory behavior, the compound selectively adsorbed *p*X over *o*X and *m*X and transformed back to its as-synthesized state, with a *p*X selectivity of 51. The authors attributed its high *p*X selectivity to the molecular imprinting effect, and additional energy barriers would arise for the adsorption of the other two isomers as they do not have the same level of shape-memory effect as *p*X.

Taking into consideration the subtle difference in molecular size and shape of the C_8 alkylaromatic hydrocarbons, kinetic or size-exclusion controlled mechanism may be implemented for their separations. Vos et al. used Cu(CDC) (CDC = trans-1,4-cyclohexanedicarboxylate) as a shape-selective adsorbent for the separation of xylene isomers.[115] The material possesses 1D channels with a diameter of 5.4 Å, which selectively adsorbed *p*X over *o*X and *m*X. It took up to 12 wt% of *p*X, but substantially lower amounts for the other two isomers under identical experimental conditions. Its capability of selective adsorption of *p*X was further evaluated by competitive adsorption measurements on mixtures of all three xylene isomers. The authors attributed the selective adsorption behavior to the suitable pore size of the MOF. Stoddart et al. reported the separation of xylene isomers by a CD-MOF (CD = cyclodextrin).[116,117] The CD-MOF was formed by the coordination of γ-CDs to alkali metal cations, which possesses transverse microporous pores. The material showed an *o*X-selective behavior with an *o*X/*m*X and *o*X/*p*X separation factors of 6.73 and 17.9, respectively. GCMC simulations attributed the preferential adsorption of *o*X to its optimal packing efficiency in the pores of the CD-MOF. The results were confirmed by another independent study,[118] which found CD-MOF-1 preferentially adsorbed *o*X over the other two xylene isomers both thermodynamically and kinetically, and its separation capability was supported by multicomponent column breakthrough measurements.

Zhu et al. developed an MOF material, In(OH)(OBA) (JUC-77, H_2OBA = 4,4′-oxybis(benzoic acid)), with rhombic channels that could efficiently separate xylene isomers.[119] The authors proposed that whether an adsorbate molecule can be adsorbed by the MOF depends on if the rectangle formed by MIN-1 (minimum dimension of the adsorbate molecule) and MIN-2 (second minimum dimension of the adsorbate molecule) could go through the rhombic channel perpendicularly. The authors found the rectangle formed by MIN-1 and MIN-2 of *p*X fit well into the rhombic channel of JUC-77, but not those of *o*X and *m*X. Their hypothesis was supported by computational simulations, and further confirmed by vapor adsorption experiments. JUC-77 showed a saturated adsorption capacity of 32 wt% of *p*X at 298 K, but it fully excluded *o*X and *m*X with essentially no adsorption under identical conditions. The selective molecular exclusion behavior of JUC-77 was attributed to its suitable channel shape and dimensions.

Separations based on selective molecular sieving are considered optimal as they offer the highest possible adsorption selectivity and superior efficiency. However, in previous examples, MOFs capable of size-exclusion separation may be very efficient in sieving out molecules larger than their pore aperture, but in most cases will adsorb unwanted molecules that are smaller than the pore aperture. Thus, they may not be suitable for effective separation of a molecule having intermediate size from a gas mixture that also contains smaller and larger molecules. In a more recent study, Zhang et al. developed an MOF, Cu_2(fbdim) (also termed as MAF-41, H_2fbdim = 2,6-ditrifluoromethyl-benzodiimidazole),[110] that shows interesting intermediate-sized molecular sieving behavior for

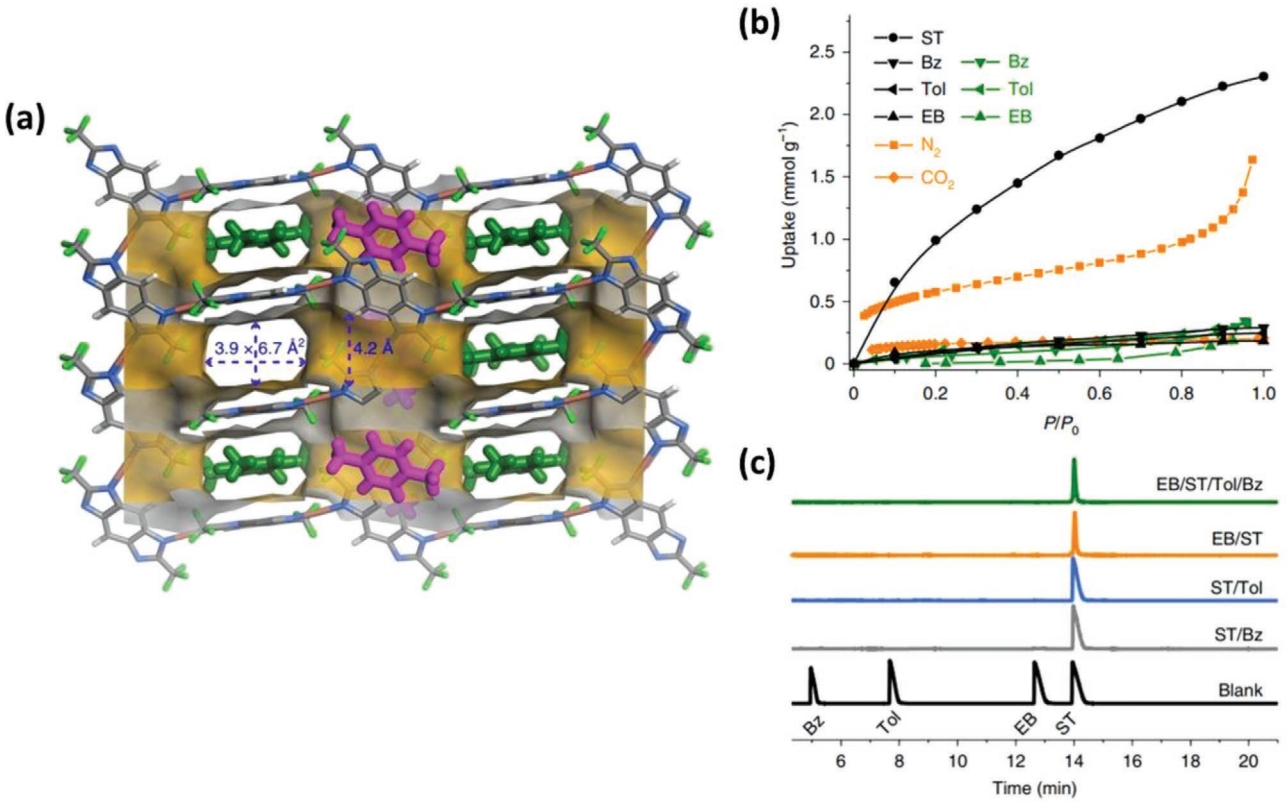

Figure 16. a) Crystal structure of pX-adsorbed MAF-41. b) Adsorption isotherms of various vapors and gases on MAF-41. c) Typical GC traces of the methanol extractions of MAF-41 after immersion in various equimolar mixtures. Reproduced with permission.[110] Copyright 2019, Springer Nature.

the separation of ST from larger and smaller analogues (EB, Tol, and Bz), an important industrial process for the production of pure ST (**Figure 16**). MAF-41 is a flexible framework that undergoes a reversible structural transformation between "open-pore state" and "closed-pore state" upon guest inclusion and removal. Interestingly, single-component adsorption experiments revealed that MAF-41 adsorbs a saturated amount of 2.31 mmol g^{-1} of ST at 298 K, but negligible EB, Tol, or Bz (less than 0.3 mmol g^{-1}). It is easy to understand the exclusion of EB as its molecular size is larger than the pore aperture of MAF-41 even in its "open-pore state," analogous to conventional selective molecular sieving. In contrast, based on in-depth computational study, the exclusion of smaller Tol and Bz was primarily a result of thermodynamic effect. The molecules have insufficient adsorption energy to induce the pore-opening, although their molecular sizes are smaller than the pore aperture of the MOF at the "open-pore state." In addition, computational simulations indicated that interaction between adsorbates (assuming residing in the pore) and the framework follows the trend of Bz < Tol << ST < EB. Gas chromatography study of the separation of EB/ST/Tol/Bz mixtures confirmed that MAF-41 is capable of extracting ST from the mixture with a purity of 99+%. The results demonstrated an interesting intermediate size sieving of ST from EB/ST/Tol with high efficiency, which can be attributed to the suitable pore aperture and restricted structural flexibility of the MOF. The uncommon selective adsorption behavior was a result of combined thermodynamic and kinetic effects.

6. Conclusion and Outlook

In this review, we have provided an overview on the recent progress of developing MOFs with optimal pore structures for the separation of industrially important hydrocarbons, with a special emphasis on separations based on size-exclusion mechanism. Over the past decade, substantial advances have been made on energy-efficient separations of various hydrocarbon mixtures by MOFs, particularly those capable of molecular sieving based separations. A number of MOF materials have outperformed traditional adsorbents as a result of exceptional tunability in their pore size, pore shape, and surface functionality. Moreover, the reticular chemistry has served as a powerful tool in guiding the structure design and porosity tuning of MOFs at sub-angstrom level, creating tailor-made MOFs with excellent separation performance.

Although tremendous progress has been made and MOFs have proven potentially useful for the separation of hydrocarbons, this research field remains underexplored with many challenges that must be addressed before MOF-based adsorptive separation technology can be industrially implemented. Some areas for improvement include: 1) Material stability: MOFs generally suffer from relatively low stability compared to conventional inorganic adsorbents. Some of them are even sensitive to air/moisture and need to be handled in a glovebox under inert atmosphere. In industrial adsorptive separations, adsorption and/or desorption processes are usually carried out at high temperature and/or high pressure to facilitate mass transfer.

Thus, adsorbents must be thermally robust and sustainable under long periods of heating. In addition, adsorbent materials must be resistant to certain impurities coexisting in the gas/vapor stream, such as moisture, H_2S, etc. While some MOF materials built on early transition metals with high valence, such as Cr^{3+} and Zr^{4+}, have demonstrated exceptional stability (e.g., MIL-101(Cr), UiO-66), continued efforts in improving the stability of MOFs are much needed, with a focus on high valence metal-based structures. 2) Separation performance: The separation performance remains unsatisfactory and requires further improvement for some important processes, such as the separation of xylenes. It is essential to achieve a suitable balance that takes into consideration both adsorption selectivity and capacity. In some cases, adsorption capacity is largely sacrificed, as a result of pore size tuning or surface functionalization, which leads to the reduction of surface area and pore volume of the materials. A possible solution is to explore MOFs with optimal pore structures that would offer high adsorption capacity as well as excellent selectivity. For example, cage-like pores as observed in ZIF-8 and Zr-MOFs with ftw topology are advantageous for separation as tuning of their pore aperture would not noticeably affect the cages resulting in high adsorption capacity. Reticular chemistry offers helpful guidelines for the optimization of pore structures and separation performance for MOFs with certain topologies. 3) Scale-up production and reduced cost: Some tailored MOF materials show optimal performance for the separation of hydrocarbons; however, they are built on organic ligands that are obtained through complicated synthesis. This leads to increased costs associated with the production of the materials, making them unfavorable for industrial implementation. In addition, the transition from small lab-scale synthesis (mg to g) to large scale synthesis (g to kg) may reduce the performance of some materials. Thus, low-cost and easily scaled-up MOFs made of simple organic linkers are much preferred.

On the other hand, the following aspects should also be considered when designing future MOFs for the separation of hydrocarbons: 1) In most early studies, kinetic diameters of adsorbates were the sole parameters considered when seeking for matching pore diameters of MOF structures. However, the examples discussed above demonstrate the importance of the shape of targeted adsorbate molecules, especially when they are much deviated from a sphere, a model used in calculating kinetic diameters. In such cases, the minimum size of the cross-section (such as the rectangle formed by MIN-1 and MIN-2) of the adsorbates should be a more reliable parameter taken into consideration. Nevertheless, this will eventually need to be verified experimentally. 2) For real-world applications, greater effort should be made to mimic the experimental conditions applied in separation industry (e.g., use of the same feed gas mixtures for real processes), which are essential for assessing the true separation performance of MOF materials. This is crucial as the MOF adsorbents may behave very differently under different conditions. For example, in the separation of ethylene and ethane, composition of the mixtures may vary significantly from different sources. Ethane-selective adsorbents may be favored for certain compositions while ethylene-selective materials can perform better with different compositions. In addition, the purification of ethylene not only involves the removal of ethane, as other impurities including methane, carbon dioxide, and C_3/C_4 paraffins/olefins may also exist in ethylene stream and need to be removed as well. Thus, the evaluation conditions should be relevant to industrial processes. Moreover, separation experiments may be performed under industrially desired temperature and pressure to fully evaluate the capability of the materials.

MOFs feature intrinsic advantages including structure diversity, high surface area/pore volume, and exceptional tunability of pore structures. Such materials have exhibited unparalleled performances and hold great promise for real-world applications such as separation of industrially important hydrocarbons, as illustrated in this review article. With continuous efforts, we are optimistic that industrial implementation of MOF-based adsorptive separation technologies for the separation of hydrocarbons may be realized in the future.

Acknowledgements

The authors thank the National Natural Science Foundation of China (No. 21901166, 21771078, and 21621001), the 111 Project (B17020), the National Key Research and Development Program of China (2016YFB0701100), Guangdong Natural Science Foundation (No. 2019A1515010692), the Scientific and Technical Innovation Council of Shenzhen (No. JCYJ20190809145615620), and the U.S. Department of Energy, Office of Science, Office of Basic Energy Sciences (award No. DE-SC0019902) for financial support.

Conflict of Interest

The authors declare no conflict of interest.

Keywords

adsorbents, adsorptive separation, hydrocarbon separation, metal–organic frameworks, size exclusion

Received: April 16, 2020
Revised: May 14, 2020
Published online:

[1] R. A. Myers, *Handbook of Petroleum Refining Processes*, McGraw-Hill, New York **2004**.
[2] V. F. D. Martins, A. M. Ribeiro, M. G. Plaza, J. C. Santos, J. M. Loureiro, A. F. P. Ferreira, A. E. Rodrigues, *J. Chromatogr. A* **2015**, *1423*, 136.
[3] D. Peralta, G. Chaplais, A. Simon-Masseron, K. Barthelet, G. D. Pirngruber, *Ind. Eng. Chem. Res.* **2012**, *51*, 4692.
[4] R. Lively, *Nature* **2016**, *532*, 435.
[5] M. Gehre, Z. Guo, G. Rothenberg, S. Tanase, *ChemSusChem* **2017**, *10*, 3947.
[6] Y. Yang, P. Bai, X. Guo, *Ind. Eng. Chem. Res.* **2017**, *56*, 14725.
[7] Y. Yang, N. Burke, S. Ali, S. Huang, S. Lim, Y. Zhu, *RSC Adv.* **2017**, *7*, 12629.
[8] Y. Li, L. Li, J. Yu, *Chem* **2017**, *3*, 928.
[9] H. Li, M. Eddaoudi, M. O'Keeffe, O. M. Yaghi, *Nature* **1999**, *402*, 276.
[10] D. Li, H.-Q. Xu, L. Jiao, H.-L. Jiang, *EnergyChem* **2019**, *1*, 100005.
[11] D. Yang, B. C. Gates, *ACS Catal.* **2019**, *9*, 1779.

[12] Y. He, W. Zhou, G. Qian, B. Chen, *Chem. Soc. Rev.* **2014**, *43*, 5657.
[13] L. Wang, Y. Han, X. Feng, J. Zhou, P. Qi, B. Wang, *Coord. Chem. Rev.* **2016**, *307*, 361.
[14] R.-B. Lin, S. Xiang, H. Xing, W. Zhou, B. Chen, *Coord. Chem. Rev.* **2019**, *378*, 87.
[15] X. Zhao, Y. Wang, D.-S. Li, X. Bu, P. Feng, *Adv. Mater.* **2018**, *30*, 1705189.
[16] M.-H. Yu, B. Space, D. Franz, W. Zhou, C. He, L. Li, R. Krishna, Z. Chang, W. Li, T.-L. Hu, X.-H. Bu, *J. Am. Chem. Soc.* **2019**, *141*, 17703.
[17] W. P. Lustig, S. Mukherjee, N. D. Rudd, A. V. Desai, J. Li, S. K. Ghosh, *Chem. Soc. Rev.* **2017**, *46*, 3242.
[18] Z. Hu, B. J. Deibert, J. Li, *Chem. Soc. Rev.* **2014**, *43*, 5815.
[19] Y. Cui, Y. Yue, G. Qian, B. Chen, *Chem. Rev.* **2012**, *112*, 1126.
[20] I. Huskić, N. Novendra, D.-W. Lim, F. Topić, H. M. Titi, I. V. Pekov, S. V. Krivovichev, A. Navrotsky, H. Kitagawa, T. Friščić, *Chem. Sci.* **2019**, *10*, 4923.
[21] A.-L. Li, Q. Gao, J. Xu, X.-H. Bu, *Coord. Chem. Rev.* **2017**, *344*, 54.
[22] W. P. Lustig, J. Li, *Coord. Chem. Rev.* **2018**, *373*, 116.
[23] H. Kaur, S. Sundriyal, V. Pachauri, S. Ingebrandt, K.-H. Kim, A. L. Sharma, A. Deep, *Coord. Chem. Rev.* **2019**, *401*, 213077.
[24] Q.-L. Zhu, Q. Xu, *Chem. Soc. Rev.* **2014**, *43*, 5468.
[25] J. Yang, Y.-W. Yang, *Small* **2020**, *16*, 1906846.
[26] H. Furukawa, K. E. Cordova, M. O'Keeffe, O. M. Yaghi, *Science* **2013**, *341*, 1230444.
[27] A. Schneemann, V. Bon, I. Schwedler, I. Senkovska, S. Kaskel, R. A. Fischer, *Chem. Soc. Rev.* **2014**, *43*, 6062.
[28] J. A. Mason, J. Oktawiec, M. K. Taylor, M. R. Hudson, J. Rodriguez, J. E. Bachman, M. I. Gonzalez, A. Cervellino, A. Guagliardi, C. M. Brown, P. L. Llewellyn, N. Masciocchi, J. R. Long, *Nature* **2015**, *527*, 357.
[29] E. J. Carrington, C. A. McAnally, A. J. Fletcher, S. P. Thompson, M. Warren, L. Brammer, *Nat. Chem.* **2017**, *9*, 882.
[30] R.-B. Lin, S. Xiang, W. Zhou, B. Chen, *Chem* **2020**, *6*, 337.
[31] J. Pei, K. Shao, L. Zhang, H.-M. Wen, B. Li, G. Qian, *Top. Curr. Chem.* **2019**, *377*, 33.
[32] D.-X. Xue, Q. Wang, J. Bai, *Coord. Chem. Rev.* **2019**, *378*, 2.
[33] W.-G. Cui, T.-L. Hu, X.-H. Bu, *Adv. Mater.* **2020**, *32*, 1806445.
[34] S. J. Geier, J. A. Mason, E. D. Bloch, W. L. Queen, M. R. Hudson, C. M. Brown, J. R. Long, *Chem. Sci.* **2013**, *4*, 2054.
[35] V. Guillerm, D. Maspoch, *J. Am. Chem. Soc.* **2019**, *141*, 16517.
[36] O. Yaghi, *MRS Bull.* **2009**, *34*, 682.
[37] H. Wang, X. Dong, V. Colombo, Q. Wang, Y. Liu, W. Liu, X.-L. Wang, X.-Y. Huang, D. M. Proserpio, A. Sironi, Y. Han, J. Li, *Adv. Mater.* **2018**, *30*, 1805088.
[38] A. Cadiau, K. Adil, P. M. Bhatt, Y. Belmabkhout, M. Eddaoudi, *Science* **2016**, *353*, 137.
[39] J.-R. Li, J. Sculley, H.-C. Zhou, *Chem. Rev.* **2012**, *112*, 869.
[40] M. Khalighi, I. A. Karimi, S. Farooq, *Ind. Eng. Chem. Res.* **2014**, *53*, 16973.
[41] J. Padin, S. U. Rege, R. T. Yang, L. S. Cheng, *Chem. Eng. Sci.* **2000**, *55*, 4525.
[42] J. Yu, L.-H. Xie, J.-R. Li, Y. Ma, J. M. Seminario, P. B. Balbuena, *Chem. Rev.* **2017**, *117*, 9674.
[43] T. K. Maji, R. Matsuda, S. Kitagawa, *Nat. Mater.* **2007**, *6*, 142.
[44] J. An, N. L. Rosi, *J. Am. Chem. Soc.* **2010**, *132*, 5578.
[45] D. N. Dybtsev, H. Chun, S. H. Yoon, D. Kim, K. Kim, *J. Am. Chem. Soc.* **2004**, *126*, 32.
[46] K.-J. Chen, D. G. Madden, T. Pham, K. A. Forrest, A. Kumar, Q.-Y. Yang, W. Xue, B. Space, J. J. Perry Iv, J.-P. Zhang, X.-M. Chen, M. J. Zaworotko, *Angew. Chem., Int. Ed.* **2016**, *55*, 10268.
[47] E. D. Bloch, W. L. Queen, R. Krishna, J. M. Zadrozny, C. M. Brown, J. R. Long, *Science* **2012**, *335*, 1606.
[48] A. M. Plonka, X. Chen, H. Wang, R. Krishna, X. Dong, D. Banerjee, W. R. Woerner, Y. Han, J. Li, J. B. Parise, *Chem. Mater.* **2016**, *28*, 1636.
[49] L. Pan, D. H. Olson, L. R. Ciemnolonski, R. Heddy, J. Li, *Angew. Chem., Int. Ed.* **2006**, *45*, 616.
[50] H. Wang, X.-L. Wang, J. Li, *ChemPlusChem* **2016**, *81*, 872.
[51] D. Banerjee, H. Wang, A. M. Plonka, T. J. Emge, J. B. Parise, J. Li, *Chem. - Eur. J.* **2016**, *22*, 11816.
[52] D. Banerjee, H. Wang, Q. Gong, A. M. Plonka, J. Jagiello, H. Wu, W. R. Woerner, T. J. Emge, D. H. Olson, J. B. Parise, J. Li, *Chem. Sci.* **2016**, *7*, 759.
[53] F.-Z. Sun, S.-Q. Yang, R. Krishna, Y.-H. Zhang, Y.-P. Xia, T.-L. Hu, *ACS Appl. Mater. Interfaces* **2020**, *12*, 6105.
[54] G.-X. Jin, X. Niu, J. Wang, J.-P. Ma, T.-L. Hu, Y.-B. Dong, *Chem. Mater.* **2018**, *30*, 7433.
[55] X. Cui, K. Chen, H. Xing, Q. Yang, R. Krishna, Z. Bao, H. Wu, W. Zhou, X. Dong, Y. Han, B. Li, Q. Ren, M. J. Zaworotko, B. Chen, *Science* **2016**, *353*, 141.
[56] P. Nugent, Y. Belmabkhout, S. D. Burd, A. J. Cairns, R. Luebke, K. Forrest, T. Pham, S. Ma, B. Space, L. Wojtas, M. Eddaoudi, M. J. Zaworotko, *Nature* **2013**, *495*, 80.
[57] T.-L. Hu, H. Wang, B. Li, R. Krishna, H. Wu, W. Zhou, Y. Zhao, Y. Han, X. Wang, W. Zhu, Z. Yao, S. Xiang, B. Chen, *Nat. Commun.* **2015**, *6*, 7328.
[58] B. Li, X. Cui, D. O'Nolan, H.-M. Wen, M. Jiang, R. Krishna, H. Wu, R.-B. Lin, Y.-S. Chen, D. Yuan, H. Xing, W. Zhou, Q. Ren, G. Qian, M. J. Zaworotko, B. Chen, *Adv. Mater.* **2017**, *29*, 1704210.
[59] J. Li, L. Jiang, S. Chen, A. Kirchon, B. Li, Y. Li, H.-C. Zhou, *J. Am. Chem. Soc.* **2019**, *141*, 3807.
[60] J. Kim, L.-C. Lin, R. L. Martin, J. A. Swisher, M. Haranczyk, B. Smit, *Langmuir* **2012**, *28*, 11914.
[61] O. T. Qazvini, R. Babarao, Z.-L. Shi, Y.-B. Zhang, S. G. Telfer, *J. Am. Chem. Soc.* **2019**, *141*, 5014.
[62] X. Wang, Y. Wu, J. Peng, Y. Wu, J. Xiao, Q. Xia, Z. Li, *Chem. Eng. J.* **2019**, *358*, 1114.
[63] H. Wu, Y. Chen, D. Lv, R. Shi, Y. Chen, Z. Li, Q. Xia, *Sep. Purif. Technol.* **2019**, *212*, 51.
[64] Y. Chen, H. Wu, D. Lv, R. Shi, Y. Chen, Q. Xia, Z. Li, *Ind. Eng. Chem. Res.* **2018**, *57*, 4063.
[65] D. Lv, R. Shi, Y. Chen, Y. Wu, H. Wu, H. Xi, Q. Xia, Z. Li, *ACS Appl. Mater. Interfaces* **2018**, *10*, 8366.
[66] Y. Chen, Z. Qiao, H. Wu, D. Lv, R. Shi, Q. Xia, J. Zhou, Z. Li, *Chem. Eng. Sci.* **2018**, *175*, 110.
[67] R.-B. Lin, H. Wu, L. Li, X.-L. Tang, Z. Li, J. Gao, H. Cui, W. Zhou, B. Chen, *J. Am. Chem. Soc.* **2018**, *140*, 12940.
[68] H. Zeng, X.-J. Xie, M. Xie, Y.-L. Huang, D. Luo, T. Wang, Y. Zhao, W. Lu, D. Li, *J. Am. Chem. Soc.* **2019**, *141*, 20390.
[69] L. Li, R.-B. Lin, R. Krishna, H. Li, S. Xiang, H. Wu, J. Li, W. Zhou, B. Chen, *Science* **2018**, *362*, 443.
[70] P.-Q. Liao, W.-X. Zhang, J.-P. Zhang, X.-M. Chen, *Nat. Commun.* **2015**, *6*, 8697.
[71] J. van den Bergh, C. Gücüyener, E. A. Pidko, E. J. M. Hensen, J. Gascon, F. Kapteijn, *Chem. Eur. J.* **2011**, *17*, 8832.
[72] C. Gücüyener, J. van den Bergh, J. Gascon, F. Kapteijn, *J. Am. Chem. Soc.* **2010**, *132*, 17704.
[73] Z. Bao, J. Wang, Z. Zhang, H. Xing, Q. Yang, Y. Yang, H. Wu, R. Krishna, W. Zhou, B. Chen, Q. Ren, *Angew. Chem., Int. Ed.* **2018**, *57*, 16020.
[74] R.-B. Lin, L. Li, H.-L. Zhou, H. Wu, C. He, S. Li, R. Krishna, J. Li, W. Zhou, B. Chen, *Nat. Mater.* **2018**, *17*, 1128.
[75] S. Yang, A. J. Ramirez-Cuesta, R. Newby, V. Garcia-Sakai, P. Manuel, S. K. Callear, S. I. Campbell, C. C. Tang, M. Schröder, *Nat. Chem.* **2015**, *7*, 121.
[76] Z. Bao, G. Chang, H. Xing, R. Krishna, Q. Ren, B. Chen, *Energy Environ. Sci.* **2016**, *9*, 3612.

[77] K. Li, D. H. Olson, J. Seidel, T. J. Emge, H. Gong, H. Zeng, J. Li, *J. Am. Chem. Soc.* **2009**, *131*, 10368.
[78] B. Zheng, G. Maurin, *Angew. Chem., Int. Ed.* **2019**, *58*, 13734.
[79] C. Y. Lee, Y.-S. Bae, N. C. Jeong, O. K. Farha, A. A. Sarjeant, C. L. Stern, P. Nickias, R. Q. Snurr, J. T. Hupp, S. T. Nguyen, *J. Am. Chem. Soc.* **2011**, *133*, 5228.
[80] J. Peng, H. Wang, D. H. Olson, Z. Li, J. Li, *Chem. Commun.* **2017**, *53*, 9332.
[81] L. Li, R.-B. Lin, X. Wang, W. Zhou, L. Jia, J. Li, B. Chen, *Chem. Eng. J.* **2018**, *354*, 977.
[82] H. Wu, Y. Yuan, Y. Chen, F. Xu, D. Lv, Y. Wu, Z. Li, Q. Xia, *AIChE J.* **2020**, *66*, e16858.
[83] D.-X. Xue, A. Cadiau, Ł. J. Weseliński, H. Jiang, P. M. Bhatt, A. Shkurenko, L. Wojtas, C. Zhijie, Y. Belmabkhout, K. Adil, M. Eddaoudi, *Chem. Commun.* **2018**, *54*, 6404.
[84] Y. Wang, N.-Y. Huang, X.-W. Zhang, H. He, R.-K. Huang, Z.-M. Ye, Y. Li, D.-D. Zhou, P.-Q. Liao, X.-M. Chen, J.-P. Zhang, *Angew. Chem., Int. Ed.* **2019**, *58*, 7692.
[85] P.-Q. Liao, N.-Y. Huang, W.-X. Zhang, J.-P. Zhang, X.-M. Chen, *Science* **2017**, *356*, 1193.
[86] M. Hartmann, S. Kunz, D. Himsl, O. Tangermann, S. Ernst, A. Wagener, *Langmuir* **2008**, *24*, 8634.
[87] M. Lange, M. Kobalz, J. Bergmann, D. Lassig, J. Lincke, J. Möllmer, A. Moeller, J. Hofmann, H. Krautscheid, R. Staudt, R. Gläser, *J. Mater. Chem. A* **2014**, *2*, 8075.
[88] H. Liu, Y. He, J. Jiao, D. Bai, D.-l. Chen, R. Krishna, B. Chen, *Chem. Eur. J.* **2016**, *22*, 14988.
[89] K. Kishida, Y. Okumura, Y. Watanabe, M. Mukoyoshi, S. Bracco, A. Comotti, P. Sozzani, S. Horike, S. Kitagawa, *Angew. Chem., Int. Ed.* **2016**, *55*, 13784.
[90] Z. Zhang, Q. Yang, X. Cui, L. Yang, Z. Bao, Q. Ren, H. Xing, *Angew. Chem., Int. Ed.* **2017**, *56*, 16282.
[91] H. Wang, J. Li, *Acc. Chem. Res.* **2019**, *52*, 1968.
[92] B. Chen, C. Liang, J. Yang, D. S. Contreras, Y. L. Clancy, E. B. Lobkovsky, O. M. Yaghi, S. Dai, *Angew. Chem., Int. Ed.* **2006**, *45*, 1390.
[93] Z. R. Herm, B. M. Wiers, J. A. Mason, J. M. van Baten, M. R. Hudson, P. Zajdel, C. M. Brown, N. Masciocchi, R. Krishna, J. R. Long, *Science* **2013**, *340*, 960.
[94] A. F. P. Ferreira, M. C. Mittelmeijer-Hazeleger, M. A. Granato, V. F. D. Martins, A. E. Rodrigues, G. Rothenberg, *Phys. Chem. Chem. Phys.* **2013**, *15*, 8795.
[95] L. Chen, S. Yuan, J.-F. Qian, W. Fan, M.-Y. He, Q. Chen, Z.-H. Zhang, *Ind. Eng. Chem. Res.* **2016**, *55*, 10751.
[96] P. A. P. Mendes, A. E. Rodrigues, P. Horcajada, C. Serre, J. A. C. Silva, *Microporous Mesoporous Mater.* **2014**, *194*, 146.
[97] N. Chang, Z.-Y. Gu, X.-P. Yan, *J. Am. Chem. Soc.* **2010**, *132*, 13645.
[98] K. Zhang, R. P. Lively, C. Zhang, R. R. Chance, W. J. Koros, D. S. Sholl, S. Nair, *J. Phys. Chem. Lett.* **2013**, *4*, 3618.
[99] P. S. Bárcia, F. Zapata, J. A. C. Silva, A. E. Rodrigues, B. Chen, *J. Phys. Chem. B* **2007**, *111*, 6101.
[100] Y. Ling, Z.-X. Chen, F.-P. Zhai, Y.-M. Zhou, L.-H. Weng, D.-Y. Zhao, *Chem. Commun.* **2011**, *47*, 7197.
[101] P. A. P. Mendes, A. E. Rodrigues, P. Horcajada, J. Eubank, T. Devic, C. Serre, J. A. C. Silva, *Adsorpt. Sci. Technol.* **2014**, *32*, 475.
[102] D. Lv, H. Wang, Y. Chen, F. Xu, R. Shi, Z. Liu, X. Wang, S. J. Teat, Q. Xia, Z. Li, J. Li, *ACS Appl. Mater. Interfaces* **2018**, *10*, 6031.
[103] A. H. Assen, Y. Belmabkhout, K. Adil, P. M. Bhatt, D.-X. Xue, H. Jiang, M. Eddaoudi, *Angew. Chem., Int. Ed.* **2015**, *54*, 14353.
[104] D.-X. Xue, Y. Belmabkhout, O. Shekhah, H. Jiang, K. Adil, A. J. Cairns, M. Eddaoudi, *J. Am. Chem. Soc.* **2015**, *137*, 5034.
[105] Y. Bai, Y. Dou, L.-H. Xie, W. Rutledge, J.-R. Li, H.-C. Zhou, *Chem. Soc. Rev.* **2016**, *45*, 2327.
[106] H. Wang, X. Dong, J. Lin, S. J. Teat, S. Jensen, J. Cure, E. V. Alexandrov, Q. Xia, K. Tan, Q. Wang, D. H. Olson, D. M. Proserpio, Y. J. Chabal, T. Thonhauser, J. Sun, Y. Han, J. Li, *Nat. Commun.* **2018**, *9*, 1745.
[107] P. A. P. Mendes, P. Horcajada, S. Rives, H. Ren, A. E. Rodrigues, T. Devic, E. Magnier, P. Trens, H. Jobic, J. Ollivier, G. Maurin, C. Serre, J. A. C. Silva, *Adv. Funct. Mater.* **2014**, *24*, 7666.
[108] H. Wang, X. Dong, E. Velasco, D. H. Olson, Y. Han, J. Li, *Energy Environ. Sci.* **2018**, *11*, 1226.
[109] l. yu, X. Dong, Q. Gong, S. R. Acharya, Y. Lin, H. Wang, Y. Han, T. Thonhauser, J. Li, *J. Am. Chem. Soc.* **2020**.
[110] D.-D. Zhou, P. Chen, C. Wang, S.-S. Wang, Y. Du, H. Yan, Z.-M. Ye, C.-T. He, R.-K. Huang, Z.-W. Mo, N.-Y. Huang, J.-P. Zhang, *Nat. Mater.* **2019**, *18*, 994.
[111] M. I. Gonzalez, M. T. Kapelewski, E. D. Bloch, P. J. Milner, D. A. Reed, M. R. Hudson, J. A. Mason, G. Barin, C. M. Brown, J. R. Long, *J. Am. Chem. Soc.* **2018**, *140*, 3412.
[112] Z. He, Y. Yang, P. Bai, X. Guo, *J. Ind. Eng. Chem.* **2019**, *77*, 262.
[113] M. Agrawal, S. Bhattacharyya, Y. Huang, K. C. Jayachandrababu, C. R. Murdock, J. A. Bentley, A. Rivas-Cardona, M. M. Mertens, K. S. Walton, D. S. Sholl, S. Nair, *J. Phys. Chem. C* **2018**, *122*, 386.
[114] X. Yang, H.-L. Zhou, C.-T. He, Z.-W. Mo, J.-W. Ye, X.-M. Chen, J.-P. Zhang, *Research* **2019**, *2019*, 9463719.
[115] J. Lannoeye, B. Van de Voorde, B. Bozbiyik, H. Reinsch, J. Denayer, D. De Vos, *Microporous Mesoporous Mater.* **2016**, *226*, 292.
[116] K. J. Hartlieb, J. M. Holcroft, P. Z. Moghadam, N. A. Vermeulen, M. M. Algaradah, M. S. Nassar, Y. Y. Botros, R. Q. Snurr, J. F. Stoddart, *J. Am. Chem. Soc.* **2016**, *138*, 2292.
[117] J. M. Holcroft, K. J. Hartlieb, P. Z. Moghadam, J. G. Bell, G. Barin, D. P. Ferris, E. D. Bloch, M. M. Algaradah, M. S. Nassar, Y. Y. Botros, K. M. Thomas, J. R. Long, R. Q. Snurr, J. F. Stoddart, *J. Am. Chem. Soc.* **2015**, *137*, 5706.
[118] L. Chen, D.-D. Zhu, G.-J. Ji, S. Yuan, J.-F. Qian, M.-Y. He, Q. Chen, Z.-H. Zhang, *J. Chem. Technol. Biotechnol.* **2018**, *93*, 2898.
[119] Z. Jin, H.-Y. Zhao, X.-J. Zhao, Q.-R. Fang, J. R. Long, G.-S. Zhu, *Chem. Commun.* **2010**, *46*, 8612.
[120] C. R. Reid, K. M. Thomas, *J. Phys. Chem. B* **2001**, *105*, 10619.
[121] C. E. Webster, R. S. Drago, M. C. Zerner, *J. Am. Chem. Soc.* **1998**, *120*, 5509.
[122] J.-R. Li, R. J. Kuppler, H.-C. Zhou, *Chem. Soc. Rev.* **2009**, *38*, 1477.